Journal of Inorganic Biochemistry 199 (2019) 110755

Contents lists available at ScienceDirect

Journal of Inorganic Biochemistry

journal homepage: www.elsevier.com/locate/jinorgbio

New mononuclear and binuclear oxomolybdenum(V) complexes containing N—N chelator: Syntheses, DFT calculations, interaction with BSA protein and in vitro cytotoxic activity

Malini Roy[a], Debanjana Biswal[a], Oiendrilla Sarkar[b], Nikhil Ranjan Pramanik[c,*], Michael G.B. Drew[d], Pritam Sadhukhan[e], Mousumi Kundu[e], Parames C. Sil[e], Syamal Chakrabarti[a,*]

[a] Department of Chemistry, University College of Science, 92, Acharya Prafulla Chandra Road, Kolkata 700009, West Bengal, India
[b] Hooghly Jyotish Chandra Vidyapith, Chinsurah, Hooghly 712101, West Bengal, India
[c] Department of Chemistry, Bidhannagar College, EB-2, Sector-1, Salt Lake, Kolkata 700064, India
[d] Department of Chemistry, The University of Reading, Whiteknights, Reading RG6 6AD, UK
[e] Division of Molecular Medicine, Bose Institute, P-1/12, CIT Scheme VII M, Kolkata 700054, India

ARTICLE INFO

Keywords:
Oxomolybdenum(V)
N-N donor ligand
DFT calculations
Protein interaction
Anticancer

ABSTRACT

A neutral bidentate ligand 2-(3-methyl-5-phenyl pyrazol-1-yl) benzthiazole (L) has been synthesized by refluxing equimolar proportions of 2-hydrazino benzthiazole and benzoyl acetone in ethanol. The ligand acts in a N—N donor fashion and forms stable mononuclear, $MoOX_3L$ [L = Ligand, X = Cl (**1**), Br (**2**)] and binuclear $Mo_2O_4X_2L_2$ [L = Ligand, X = Cl (**3**), Br (**4**)] complexes with molybdenum(V). The ligand and complexes are thoroughly characterized by elemental analyses, IR, UV–Vis spectroscopy, EPR study, magnetic susceptibility, thermogravimetry and cyclic voltammetry. Magnetic moment measurements reveal that the mononuclear complexes are paramagnetic while the binuclear complexes are diamagnetic in nature. EPR studies also confirm the presence of a mononuclear Mo(V) moiety in the complexes. Relevant Density Functional Theory (DFT) calculations have been carried out to determine the structures of the synthesized compounds. The binding mode and mechanism of interaction of the synthesized compounds with bovine serum albumin (BSA) were studied by concentration dependent absorption and fluorescence titration experiments. The ligand and complexes **1–4** are screened for their potential in vitro anticancer activities against three different human cancer cell lines, namely, cervix adenocarcinoma epithelial cells (HeLa), renal carcinoma cells (SK-RC-45) and breast adenocarcinoma cells (MCF-7). The oxomolybdenum(V) complexes are found to exhibit higher anticancer potency towards the cancer cells than the free ligand. Also, structure activity relationship (SAR) studies of this new series of oxomolybdenum(V) complexes indicate that the anticancer activity is to some extent dependent on the electronic effects of the halogen atom coordinated to the molybdenum centre.

1. Introduction

Molybdenum belongs to the second transition metal series in the chromium family. The chemistry of molybdenum has received considerable interest because of its large number of accessible oxidation states ranging from −2 to +6, the presence of molybdenum in metalloenzymes and its significant role in hydroxylase and oxotransferase enzymes [1–7]. Molybdenum can form stable complexes with a large variety of ligands in its higher oxidation states +IV, +V and +VI. Over the decades, Mo(VI) complexes have been extensively studied due to their stable electronic arrangement. Comparatively, Mo(V) complexes have been less discussed due to their instability. The chemistry of Mo (V) is dominated by the paramagnetic mononuclear molybdenyl cation MoO^{3+} and diamagnetic binuclear oxo-bridged $Mo_2O_3^{4+}$ or $Mo_2O_4^{2+}$ cores [8–14].

The treatment and eradication of cancer involves chemotherapy as one of the important techniques [15]. Due to the several drawbacks of current anticancer drugs [16], the identification of new therapies is a domain of relevance in biomedical research. Molybdenum plays an important role in biology [17] and hence it's utility in the field of pharmaceutical chemistry demands exploration.

The donor set and the ligand environment surrounding

* Corresponding authors.
E-mail addresses: nr_pramanik@yahoo.co.in (N.R. Pramanik), schakrabarti2014@gmail.com (S. Chakrabarti).

https://doi.org/10.1016/j.jinorgbio.2019.110755
Received 14 February 2019; Received in revised form 21 June 2019; Accepted 24 June 2019
Available online 25 June 2019
0162-0134/

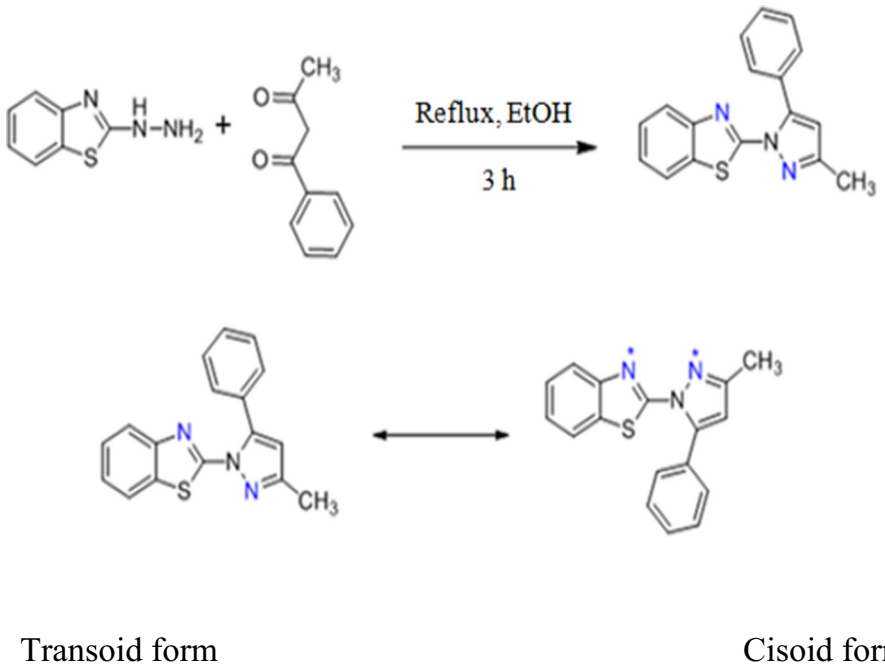

Scheme 1. Reaction diagram for isolation of the ligand.

molybdenum often influence important factors such as solubility, oxidation state and reactivity of the complexes. Molecules containing thiazole ligands are widespread in nature possessing a myriad of biological applications involving their anticancer, antiviral, antibacterial and anti-inflammatory properties [18]. Hence, the thiazole template is a privileged structural fragment in medicinal chemistry. Benzthiazoles represent a class of heterocyclic compounds of keen interest to medicinal chemists [19–23]. They play an important role in chemistry and attract continuing interest due to their diverse biological activities viz. anticancer [24], antimicrobial [25], antiviral [26], antimalarial [27], analgesic [28], anti-inflammatory [29], antidiabetic [30] and fungicidal [31]. Benzthiazole compounds exhibit anticancer effects mostly by inducing protein expression and DNA damage [32]. Molybdenum complexes with potential N—N donor ligands containing a benzthiazole nucleus have been reported [33]. Complexes of metals other than molybdenum and ligands derived from benzthiazole and 2-pyridyl derivatives have also been studied earlier [34,35]. Substituted pyrazoles also have a promising role as anticancer [36], antifungal [37,38], insecticidal [39] and effective antibacterial agents [40].

Consideration of these facts combined with the pharmacological properties of molybdenum, indicated that oxomolybdenum(V) complexes containing thiazole and pyrazole moieties within the ligand framework could be of great medicinal interest.

It is important to identify the affinity or interaction of metallodrugs towards serum albumins (SA), a carrier protein, because SAs often aid the transportation of drugs through the bloodstream to cells and tissues. Among the serum albumin proteins, bovine serum albumin (BSA) has wide applications in the pharmaceutical field due to its low cost, high availability and structural homology with human serum albumin (HSA) [41].

This work reports the coordination behaviour of the bidentate chelating ligand 2-(3-methyl-5-phenyl pyrazol-1-yl) benzthiazole (L) towards the oxomolybdenum(V) centre. We have synthesized both mononuclear and binuclear complexes **1–4** of the general formula $MoOX_3L$ and $Mo_2O_4X_2L_2$ (where L = Ligand, X = Cl, Br). The synthesized complexes are thoroughly characterized by elemental analyses, IR, UV–Vis spectroscopy, EPR study, magnetic susceptibility, thermogravimetry and cyclic voltammetry. Structurally characterized oxomolybdenum(V) complexes with this type of ligands are rare, so supportive Density Functional Theory (DFT) calculations were carried out to establish the probable structures of the complexes. BSA binding efficiencies of the ligand and complexes were monitored by concentration dependent absorption and steady state fluorescence titration studies. The results show that all of the compounds could quench the intrinsic fluorescence of BSA in a static quenching process. To evaluate the potential usefulness of the ligand and oxomolybdenum(V) complexes **1–4** as anticancer agents, a panel of human cancer cell lines of different origin [e.g. renal carcinoma cells (SK-RC-45), breast adenocarcinoma cells (MCF-7) and cervix adenocarcinoma epithelial cells (HeLa)] was used. The encouraging results reported herein highlight the potential of these oxomolybdenum(V) complexes to act as prospective anticancer metallodrugs and are also useful to understand the factors that are responsible for their activities.

2. Materials and methods

2.1. Materials

Reagent grade solvents were dried and distilled prior to use. All other chemicals used for preparative work were of reagent grade, available commercially and used without further purification.

2.2. Synthesis

2.2.1. Synthesis of the ligand (L)

1.53 g of 2-hydrazino benzthiazole (10.0 mmoL) and 1.62 g benzoyl acetone (10.0 mmoL) were dissolved in ethanol. The solution was refluxed for 3 h (Scheme 1). White needle shaped crystalline compound was obtained from the solution. The compound was filtered, washed with ethanol and dried over fused $CaCl_2$. M.P. 146 °C; Yield: 80%. Anal. Calcd. for $C_{17}H_{13}N_3S$ (%): C, 70.10; H, 4.47; N, 14.43. Found: C, 70.09; H, 4.43; N, 14.35. IR (KBr Pellet), cm^{-1}: $\nu_{(C=N)}$ 1562(s); ^1H NMR ($CDCl_3$): (CH_3-C) 2.40 s (3H), (Aromatic protons) 6.32–7.78 m (10H). ESI-MS (+) in MeOH: *m/z* 292 (M + H) and *m/z* 314 (M + 23).

2.2.2. Synthesis of the complexes

2.2.2.1. Oxotrichloro-[2-(3-methyl-5-phenyl pyrazol-1-yl) benzthiazole] molybdenum(V) $MoOCl_3L$ (1). 0.50 g molybdenum trioxide (3.5

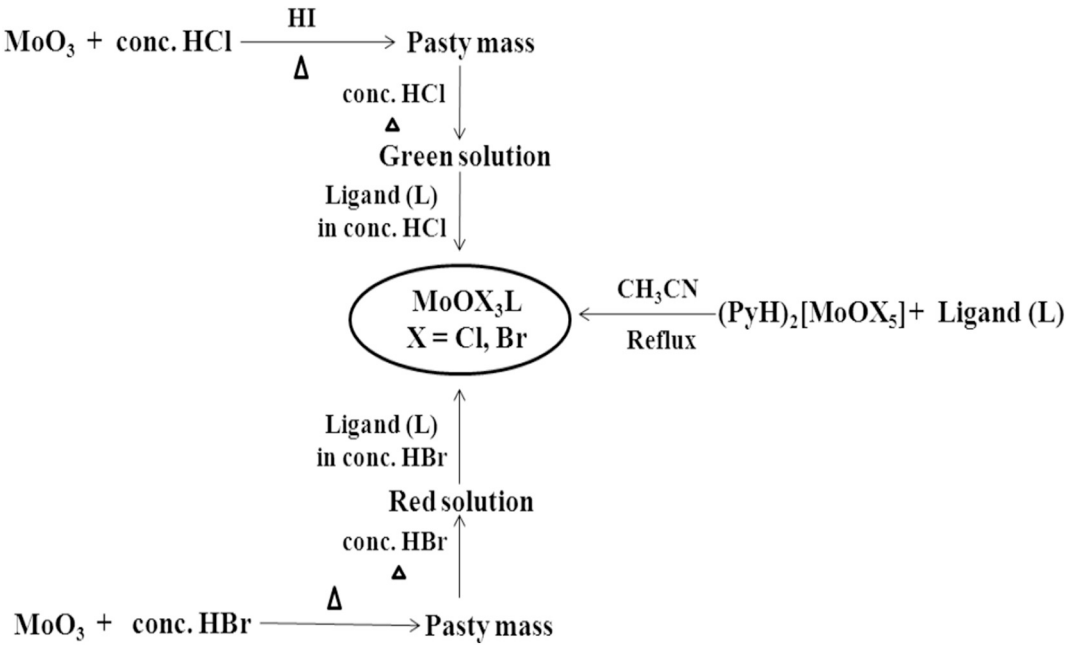

Scheme 2. Reaction diagram for the synthesis of $MoOX_3L$ complexes [X = Cl (**1**), Br (**2**)].

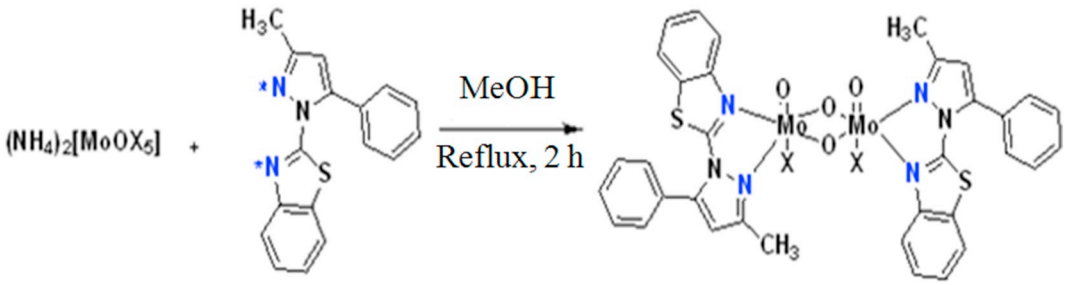

Scheme 3. Reaction diagram for the synthesis of $Mo_2O_4X_2L_2$ complexes [X = Cl (**3**), Br (**4**)].

mmoL) was dissolved in 10 mL concentrated HCl with vigorous stirring. 10 drops of HI was added to the mixture. Then it was heated to boiling to eliminate the liberated I_2 completely until a pasty mass was obtained which was subsequently redissolved in another 10 mL of concentrated HCl while heating. The resulting green solution was cooled to room temperature, then 1.02 g (3.5 mmoL) of the ligand 2-(3-methyl-5-phenyl pyrazol-1-yl) benzthiazole previously dissolved in a minimum quantity of concentrated HCl was added in ice-cold conditions with stirring. A light yellow compound was separated out, filtered, washed with concentrated HCl and dried in vacuum over solid KOH (Scheme 2). Anal. Calcd. for $C_{17}H_{13}N_3SOCl_3Mo$ (%): C, 40.04; H, 2.55; N, 8.24; Mo, 18.84, Found: C, 40.14; H, 2.51; N, 8.19; Mo, 18.38; IR (KBr Pellet), cm^{-1}: $\nu_{(C=N)}$ 1508(s), $\nu_{(Mo=O)}$ 948(s), $\nu_{(Mo-N)}$ 557(m); UV–Vis (CH_2Cl_2) [λ_{max}/nm ($\varepsilon/M^{-1}cm^{-1}$)]: 232 (1026), 287 (1198), 366 (260), 731 (55); ESI-MS (+) in MeOH: *m/z* 510 (M + H).

*2.2.2.2. Oxotribromo-[2-(3-methyl-5-phenyl pyrazol-1-yl) benzthiazole] molybdenum(V) $MoOBr_3L$ (**2**).* 0.50 g (3.5 mmoL) molybdenum trioxide was dissolved in 5 mL concentrated HBr with stirring. The liberated bromine was completely boiled off to obtain a pasty mass which was then redissolved in another fresh 10 mL concentrated HBr on a heating mantle. The resulting red solution was cooled to room temperature and 1.02 g (3.5 mmoL) of the ligand 2-(3-methyl-5-phenyl pyrazol-1-yl) benzthiazole, previously dissolved in minimum quantity of concentrated HBr, was added in an ice-bath with stirring. An orange coloured compound was formed which was filtered, washed with HBr and dried in a vacuum desiccator over solid KOH (Scheme 2). Anal. Calcd. for $C_{17}H_{13}N_3SOBr_3Mo$ (%): C, 31.73; H, 2.02; N, 6.53; Mo, 14.93, Found: C, 31.62; H, 2.10; N, 6.51; Mo, 15.02; IR (KBr Pellet), cm^{-1}: $\nu_{(C=N)}$ 1507(s), $\nu_{(Mo=O)}$ 944(s), $\nu_{(Mo-N)}$ 557(m); UV–Vis (CH_2Cl_2) [λ_{max}/nm ($\varepsilon/M^{-1}cm^{-1}$)]: 234 (1610), 304 (1660), 749 (99); ESI-MS (+) in MeOH: *m/z* 645 (M + 2H).

Complexes **1** and **2** can also be prepared in a different way by refluxing the ligand (0.29 g) and the corresponding $(PyH)_2[MoOCl_5]$ (0.45 g) or $(PyH)_2[MoOBr_5]$ (0.67 g) in equimolar proportions in dry acetonitrile for 2 h.

*2.2.2.3. Oxo-μ-dioxochlorobis-[2-(3-methyl-5-phenyl pyrazol-1-yl) benzthiazole]molybdenum(V) $Mo_2O_4Cl_2L_2$ (**3**).* A mixture of 0.33 g $(NH_4)_2[MoOCl_5]$ (1.0 mmoL) and 0.29 g of the ligand 2-(3-methyl-5-phenyl pyrazol-1-yl) benzthiazole (1.0 mmoL) was refluxed in methanol for 2 h. A pink microcrystalline compound was separated out from the filtered solution, washed with methanol and dried in a vacuum desiccator over solid KOH (Scheme 3). Anal. Calcd. for $C_{34}H_{26}N_6S_2O_4Cl_2Mo_2$ (%): C, 44.93; H, 2.86; N, 9.25; Mo, 21.14, Found: C, 44.85; H, 2.72; N, 9.31; Mo, 20.98; IR (KBr Pellet), cm^{-1}: $\nu_{(C=N)}$ 1517(s), $\nu_{(Mo=O)}$ 976(s), $\nu_{(Mo-N)}$ 693(s); $\nu_{(Mo\text{-}O\text{-}Mo)}$ 758(s); UV–Vis (CH_2Cl_2) [λ_{max}/nm ($\varepsilon/M^{-1}cm^{-1}$)]: 233 (1360), 295 (880), 491 (414); ESI-MS (+) in MeOH: *m/z* 910 (M + H).

*2.2.2.4. Oxo-μ-dioxobromobis-[2-(3-methyl-5-phenyl pyrazol-1-yl) benzthiazole]molybdenum(V) $Mo_2O_4Br_2L_2$ (**4**).* A mixture of 0.55 g $(NH_4)_2[MoOBr_5]$ (1.0 mmoL) and 0.29 g of the ligand 2-(3-methyl-5-phenyl pyrazol-1-yl) benzthiazole (1.0 mmoL) was refluxed in methanol

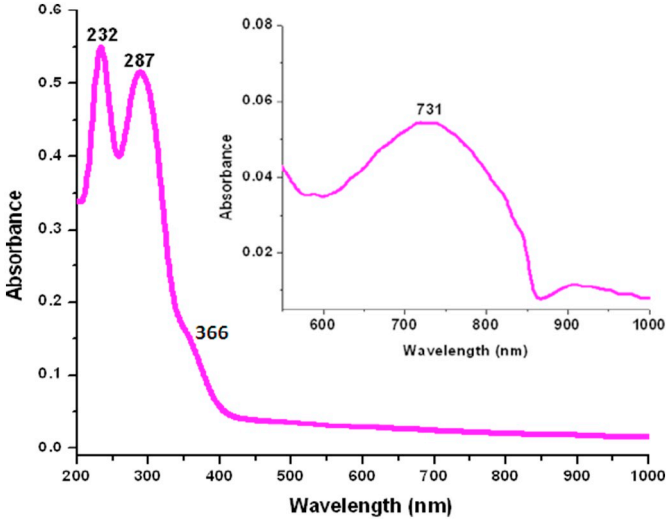

Fig. 1. UV-Spectra of complex **1** in dry dichloromethane solvent at room temperature. Inset: peak in the visible region is obtained at high complex concentration.

for 2 h. The product was separated out from the solution after cooling. It was filtered, washed with methanol and dried in a vacuum desiccator over solid KOH (Scheme 3). Anal. Calcd. for $C_{34}H_{26}N_6S_2O_4Br_2Mo_2$ (%): C, 40.88; H, 2.60; N, 8.42; Mo, 19.24, Found: C, 40.79; H, 2.55; N, 8.21; Mo, 19.01; IR (KBr Pellet), cm^{-1}: $\nu_{(C=N)}$ 1516(s), $\nu_{(Mo=O)}$ 975(vs), $\nu_{(Mo-N)}$ 693(s); $\nu_{(Mo\text{-}O\text{-}Mo)}$ 758(s); UV–Vis (CH_2Cl_2) [λ_{max}/nm (ε/$M^{-1}\,cm^{-1}$)]: 230 (1560), 260 (1260), 319 (1190); ESI-MS (+) in MeOH: *m/z* 999 (M + H).

Unfortunately, despite many attempts, no suitable single crystals of any of the complexes could be obtained for X-ray diffraction.

2.3. Physical measurements

Elemental analyses were performed on a Perkin-Elmer 240C, H, N analyzer. IR spectra were recorded as KBr pellets on a Perkin-Elmer model 883 infrared spectrophotometer. Electronic spectra were recorded using a HITACHI U-3501 UV–Vis recording spectrophotometer. Magnetic susceptibility was measured with a PAR model 155 vibrating sample magnetometer with Hg [$Co(SCN)_4$] as calibrant. Electrochemical data were collected on a Sycopel model AEW2 1820 F/S instrument at 298 K using a Pt working electrode, Pt auxiliary electrode and SCE reference electrode. Cyclic voltammograms were recorded in DMF containing 0.1 M TBAP as supporting electrolyte. Thermal analyses were carried out in a NETZSCH STA 449 *F3 Jupiter* thermal Analyzer in a dynamic atmosphere of dinitrogen (flow rate = 30 $cm^3\,min^{-1}$). EPR spectra were recorded at room temperature using a Varian V-4502 ESR Spectrophoto meter keeping the frequency at 9.3 GHz. Mass spectra were recorded by a Waters XIVO GTS QTOF spectrometer.

2.4. DFT calculations

Calculations were carried out using the Gaussian 03 program [42]. Structures were optimized using the UB3LYP density functional together with basis sets LANL2DZ for Mo, Br; 6-31 + G* for S, Cl; and 6-31G for the remaining atoms C, H, N and O.

2.5. Protein interaction study

2.5.1. Absorption study of the compounds with BSA protein

Bovine serum albumin (BSA) was purchased from Sigma-Aldrich. A stock solution of BSA (10^{-5} M) was prepared by dissolving calculated amount of BSA in phosphate buffer (pH = 7) and preserved at 4 °C for further use. Stock solutions of the compounds were prepared in ethanol maintaining the concentration 10^{-4} M. Absorption spectra were recorded using a Hitachi U-3501 UV–Vis spectrophotometer. BSA (2 mL, 10^{-5} M) was titrated with successive additions of the compounds (0–20 μL) using a micropipette.

2.5.2. Fluorescence quenching study of the compounds with BSA protein

To investigate the interaction between BSA and the synthesized compounds, emission spectra were recorded on a PerkinElmer LS55 fluorescence spectrometer with rectangular quartz cuvette of 1 cm path length at a fixed excitation wavelength corresponding to BSA at 275 nm and monitoring the emission at 356 nm at room temperature. The excitation and emission slit widths and scan rates were constantly maintained for all the experiments. 2 mL BSA solution (10^{-5} M) was titrated by successive addition of 10^{-4} M compound solution (0–20 μL).

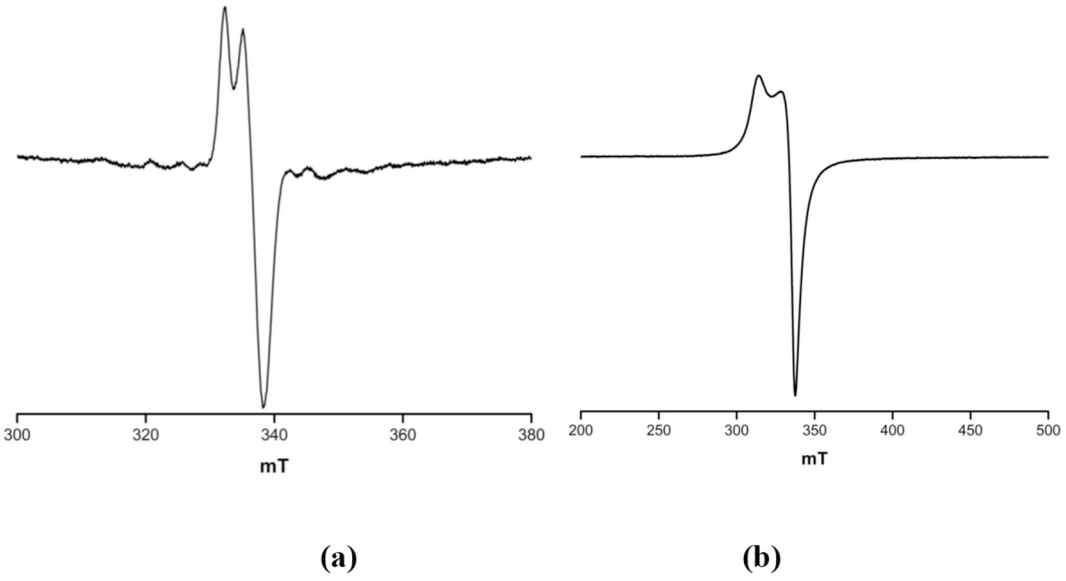

Fig. 2. EPR spectra of (a) complex **1** and (b) complex **2** at room temperature.

Table 1
EPR spectral data of complexes **1** and **2** at room temperature.

Complexes	$g_{\parallel}$ (G)	$g_{\perp}$(G)	< g > (G)
$MoOCl_3L$ (**1**)	1.94	1.96	1.95
$MoOBr_3L$ (**2**)	1.96	1.99	1.98

Table 2
Cyclic voltammetric results[a] (V vs SCE) for the complexes **1-4** at 298 K.

Complexes	E_{pa} (V)	E_{pc} (V)	
	Mo^{V}/Mo^{VI}	Mo^{VI}/Mo^{V}	Mo^{V}/Mo^{IV}
$MoOCl_3L$ (**1**)	+1.13	−0.43	−1.16
$MoOBr_3L$ (**2**)	+0.69	−0.53	−0.96
$Mo_2O_4Cl_2L_2$ (**3**)	+1.63	−0.39	−0.74
$Mo_2O_4Br_2L_2$ (**4**)	+0.70	−0.74	−1.54

[a] *Solvent*: DMF (dry, degassed); supporting electrolyte: 0.1 M TBAP; solution strength: 10^{-3} M; working electrode: platinum; reference electrode: SCE; scan rate: 200 mVs^{-1}.

2.6. Anticancer activity

2.6.1. Cell culture

In the present study, three different cancer cell lines namely, human cervix adenocarcinoma epithelial cells (HeLa), human renal cell carcinoma (SK-RC-45), human breast adenocarcinoma cells (MCF-7) and human normal kidney epithelial cells (NKE cells) are used. The cell lines were obtained from NCCS, Pune, India. The cells were cultured in a T-75 flask with RPMI-1640 medium (for SK-RC-45, MCF-7 and NKE) or DMEM (for HeLa) supplemented with fetal bovine serum (FBS) and antibiotics at 37 °C in a humidified incubator with 5% CO_2.

2.6.2. Determination of the cytotoxic potential

Cytotoxic potentials of the ligand and oxomolybdenum(V) complexes **1–4** were determined by MTT cell viability assays following the methods of Saha et al [43]. The cultured cells were seeded in a 24-well culture plate at a concentration of 4×10^4 cells with 500 µL media in each well. The five compounds were dissolved separately in phosphate buffered saline (PBS) and added to the cells. Control cells were treated with PBS only. After exposure for 24 h, the media was discarded and the cells were washed gently with PBS. 1 mL of MTT stock solution (5 mg/mL) was diluted into 10 mL serum-free media and added to each well. The plate was then incubated at 37 °C for 4 h. 500 µL DMSO was added in each well to dissolve the formazan crystals. The plate was gently shaken for 10 min to dissolve the precipitation. Finally, the absorbance was measured in a spectrophotometer at 570 nm.

2.6.3. Determination of the mode of cell death

FACS analysis was performed to investigate the mode of cell death induced by the ligand and oxomolybdenum(V) complexes. The experimental cells were cultured in 6-well plates and incubated with different compounds in separate wells. After 24 h treatment, the cells were scraped and centrifuged at room temperature (2000 rpm, 5 min). The cell pellets were washed with PBS and were resuspended in Annexin V Binding Buffer to which 1 µL of Annexin V/FITC was added and incubated for 5 min in dark (at room temperature). Immediately after incubation, the samples were analyzed flow cytometrically in FACS Verse with an excitation wavelength of 488 nm and emission wavelength of 520 nm [44].

2.6.4. Determination of the intracellular ROS

The intracellular ROS levels were determined to investigate the effect of the ligand and oxomolybdenum(V) complexes on intracellular redox environment. The analyses were performed following the protocol as described elsewhere [45]. Approximately 2×10^6 cells were plated and exposed to the compounds for specified dose and time. After incubation, the cells were first scraped and then pelleted by centrifugation (300*g*, 5 min, room temperature). Then the cells were resuspended in 1 mL of PBS and H_2DCFDA was added at a final concentration of 2 µM. After that the cells were subjected to incubation in the dark for 20 min at 37 °C. Finally, the analyses were carried out with FACS Verse at an excitation wavelength of 488 nm and emission wavelength of 520 nm.

2.6.5. Determination of the lipid peroxidation

Lipid peroxidation was determined by estimating the level of malondialdehyde (MDA) in the cells to ensure the occurrence of oxidative stress. Briefly, the control and treated cells were collected and subjected to sonication from different experimental groups. Each of the sonicated samples was then mixed with 20% trichloro acetic acid and 0.67% thiobarbituric acid. The mixtures were then heated at 100 °C for 1 h and kept in an ice bucket for cooling. Finally, centrifugation was done and the absorbance of the supernatant was measured at 535 nm using a spectrophotometer [46].

2.6.6. Determination of the cellular morphology

To analyze the cellular morphology of the SK-RC-45 cells upon the exposure of complex **4**, phase contrast microscopic imaging was done. The cells were plated in 6-well culture dish and after overnight incubation the cells were exposed to complex **4**. The cells were observed at an interval of 6 h and micrographs were taken under 10× magnification using a phase contrast microscope.

2.6.7. Determination of the DNA fragmentation

In order to determine the mode of cell death in the SK-RC-45 cells

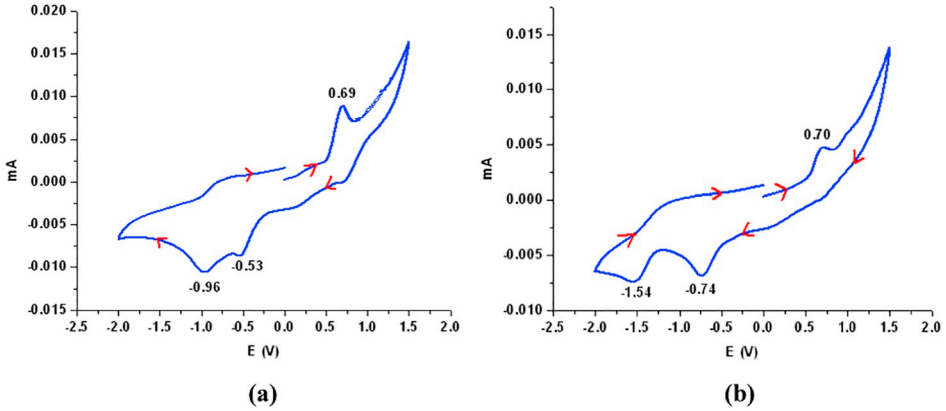

Fig. 3. Cyclic voltammograms of (a) complex **2** and (b) complex **4** in DMF at 298 K.

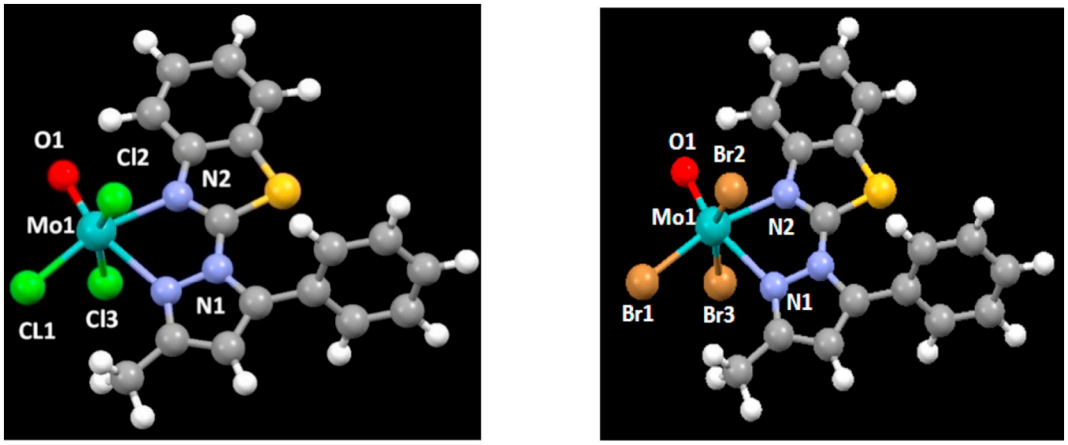

Fig. 4. Optimized molecular structures of (a) complex **1** and (b) complex **2**.

Table 3
Dimensions (distances, Å; angles, deg) in the coordination spheres of complexes **1** and **2**.

	1 (X = Cl)	**2** (X = Br)
Mo(1)-X(1)	2.353	2.557
Mo(1)-X(2)	2.4154	2.621
Mo(1)-X(3)	2.401	2.611
Mo(1)-O(1)	1.683	1.680
Mo(1)-N(1)	2.455	2.444
Mo(1)-N(2)	2.262	2.252
X(1)-Mo(1)-X(2)	91.12	91.57
X(1)-Mo(1)-X(3)	91.31	91.94
X(2)-Mo(1)-X(3)	158.78	159.44
O(1)-Mo(1)-X(1)	104.29	102.57
O(1)-Mo(1)-X(2)	99.21	98.89
O(1)-Mo(1)-X(3)	100.60	100.10
O(1)-Mo(1)-N(1)	162.88	162.85
O(1)-Mo(1)-N(2)	94.30	93.86
X(1)-Mo(1)-N(1)	92.72	94.53
X(1)-Mo(1)-N(2)	161.41	163.58
X(2)-Mo(1)-N(1)	78.98	79.09
X(2)-Mo(1)-N(2)	85.42	85.47
X(3)-Mo(1)-N(1)	80.64	80.44
X(3)-Mo(1)-N(2)	85.59	86.46
N(1)-Mo(1)-N(2)	68.89	69.04

upon exposure of complex **4**, the cells were observed under fluorescent microscope following DAPI staining. DAPI is a fluorescent DNA binding dye which binds to the DNA at AT rich region. For the microscopic analysis the cells were plated in a 6-well culture dish (upon a coverslip). After the exposure of complex **4** for 24 h, the cells were washed with 1× PBS and the coverslips were mounted on a glass slide with a mounting media containing DAPI. The coverslips were sealed with nail polish and dried for 15 min in dark. The slides were observed under 20× objective with an excitation at 358 nm (UV) and emission at 461 nm (blue).

2.6.8. Colony forming assays

Colony forming assays were performed according to the protocol as described elsewhere [47]. Briefly, 0.3×10^6 cells were plated in a culture dish and were treated with the complex **4** for 24 h. After treatment, the cells were subjected to trypsinization and again plated under normal culture conditions in RPMI supplemented in 10% FBS. The culture dish was then incubated for 2 weeks. Finally, the cells were washed twice with PBS and stained with the staining solution (0.5% crystal violet solution containing 6.0% glutaraldehyde). The culture dish was then photographed and quantified using the Image J software [47].

3. Results and discussion

3.1. Synthesis

The neutral bidentate ligand was prepared by refluxing equimolar amount of 2-hydrazino benzthiazole and benzoyl acetone in ethanol medium. The ligand was satisfactorily characterized by elemental analyses, IR, ^{1}H NMR and mass spectra.

The mononuclear Mo(V) complexes **1** and **2** have been prepared by mixing a solution of MoO^{3+} and the ligand in 1:1 molar proportion at ice cold condition in 12 N HCl and 9 N HBr medium respectively. The binuclear complexes **3** and **4** have been synthesized by refluxing equimolar proportion of ammonium oxopentahalomolybdate $(NH_4)_2[MoOX_5]$ and the ligand by using methanol as solvent. Complexes **1** and **2** were found to be paramagnetic due to presence of d^1 configuration while the other two binuclear complexes **3** and **4** were diamagnetic [48]. All the complexes have been successfully characterized by elemental analyses, IR, electronic spectra, EPR, thermogravimetry and cyclic voltammetry. The molecular formulation and some structural information can be obtained from ESI-MS analysis and elemental analysis. DFT calculations of the complexes have also been carried out. All the synthesized compounds have been analyzed for their chemical and biological consequences.

3.2. IR spectra

Characteristic IR bands of the ligand and the complexes **1–4** are given in the experimental section and the representative diagrams are shown in Fig. S1. The IR spectra of the ligand exhibits a strong band at around 1562 cm^{-1} and assigned to $\nu_{(C=N)}$ stretching mode [49]. In the corresponding complexes, this band is red shifted to1507 to 1517 cm^{-1} indicating coordination of two N atoms [33] to metal ion. All the complexes possess a very strong band in 944 cm^{-1} to 976 cm^{-1} region due to $\nu_{(Mo=O)}$ stretching vibration [33,50]. A band with medium intensity is observed around 557 cm^{-1} to 693 cm^{-1} range which is attributed to $\nu_{(Mo-N)}$ mode [51]. The binuclear complexes (**3** and **4**) exhibit strong bands around 758 cm^{-1} due to $\nu_{(Mo\text{-}O\text{-}Mo)}$ bridging [33,52] which are absent in the corresponding mononuclear complexes (**1** and **2**).

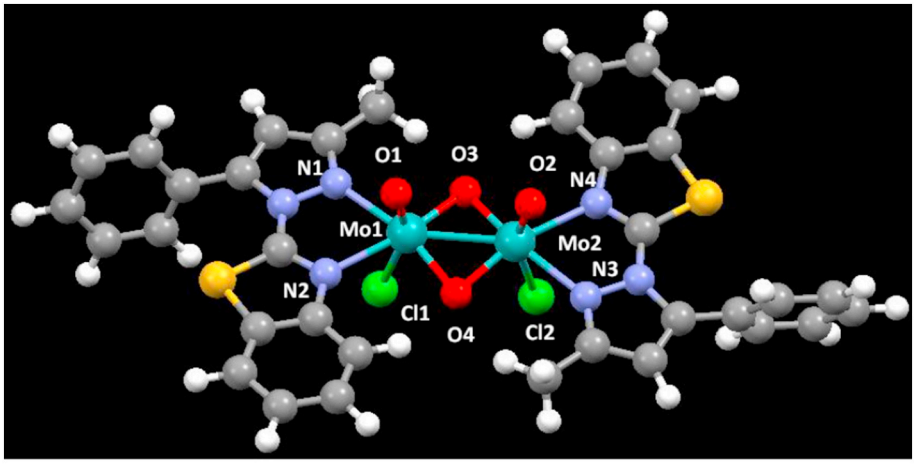

(a)

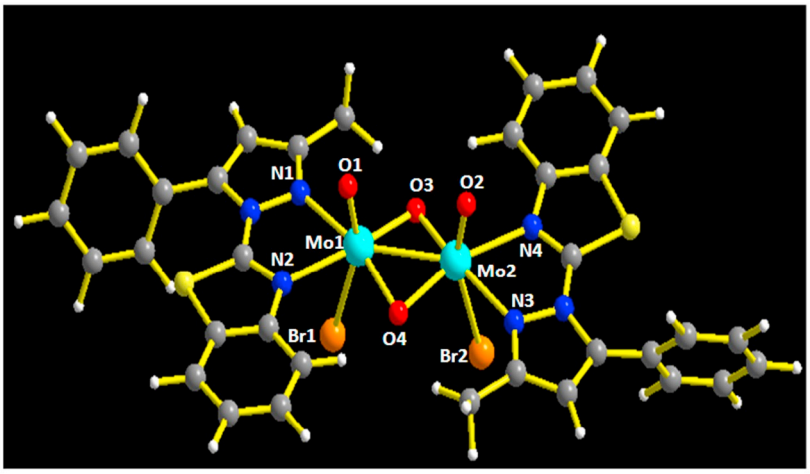

(b)

Fig. 5. Optimized molecular structure of (a) complex **3** and (b) complex **4**.

3.3. Electronic spectra

Molybdenum(V) ion is d^1 electron system with free ion term ^2D. In an octahedral crystal field, this electron occupies lower energy t_{2g} level and gives rise to the ground state term $^2T_{2g}$. In the mononuclear [MoO^{3+}] complexes of Mo(V), due to unsymmetrical alignment of Mo═O bond along the axis, the site symmetry is lowered and t_{2g} splits into $^2B_2$ (d_{xy}), ^2E (d_{xz},d_{yz}) and e_g splits into $^2B_1$($d_{x^2-y^2}$) and $^2A_1$(d_{z^2}). Hence, three electronic transitions are expected of which the third one $^2B_2 \rightarrow {}^2A_1$ is obscured by higher intensity peaks of LMCT bands [48].

The electronic spectra of the oxomolybdenum(V) complexes **1–4** have been recorded in dry dichloromethane and the spectral data are given in the experimental section. All the complexes display intense absorption bands in the range of 295–366 nm, which is attributed to L ($p\pi$) → Mo($d\pi$) LMCT transitions involving filled HOMO of the ligand to empty LUMO of molybdenum [53,54]. The strong absorption bands in the range 260–287 nm and 230–234 nm may be assigned to $^2B_2 \rightarrow {}^2B_2$ (I) and $^2B_2 \rightarrow {}^2B_2$ (II) respectively. The complexes **1** and **2** possess a characteristic band in the visible region 731 nm to 749 nm due to d-d transition ($^2B_2 \rightarrow {}^2E$) which confirms the presence of mononuclear Mo (V) centre in the complexes [55] Fig. 1. On the other hand, this particular band is absent in the complexes **3** and **4** which is further evidence that the complexes are diamagnetic in nature [56].

3.4. EPR spectra

EPR spectroscopy gives information about the nuclearity and electronic structures of a paramagnetic compound. X-band EPR spectra of the complexes **1** and **2** were recorded in dichloromethane at room temperature. The complexes give rise to two well resolved single lines only (Fig. 2) and the spectral parameters are given in the Table 1. The $g_\parallel < g_\perp$ relationship was observed corresponding to an axially compressed d_{xy}^1 configuration [56]. The < g > values indicate that the complexes **1** and **2** are mononuclear with Mo(V) moiety.

3.5. Magnetic susceptibility

Magnetic moments of the two synthesized mononuclear oxomolybdenum(V) complexes (**1** and **2)** are in the range of 1.58 and 1.67 B.M. respectively at room temperature indicating the presence of octahedral configuration with one unpaired electron in accordance with spin-only value of the d^1 system of Mo(V) centre [57–59]. This is indicative of effective quenching of orbital angular momentum by a low symmetry ligand field surrounding the metal. The complexes

Table 4
Dimensions (distances, Å; angles, deg) in the coordination spheres of complexes **3** and **4**.

Bond distances	**3** (X = Cl)	**4** (X = Br)	Bond angles	**3** (X = Cl)	**4** (X = Br)
Mo(1)-Mo(2)	2.597	2.580	O(1)-Mo(1)-X(1)	156.60	154.59
Mo(1)-O(1)	1.708	1.710	O(1)-Mo(1)-N(1)	83.86	84.89
Mo(1)-X(1)	2.523	2.771	O(1)-Mo(1)-N(2)	81.87	82.14
Mo(1)-N(1)	2.336	2.306	O(1)-Mo(1)-O(3)	104.05	104.41
Mo(1)-N(2)	2.354	2.332	O(1)-Mo(1)-O(4)	103.78	104.42
Mo(1)-O(3)	1.950	1.946	X(1)-Mo(1)-N(1)	76.61	75.93
Mo(1)-O(4)	1.949	1.950	X(1)-Mo(1)-N(2)	76.56	75.77
Mo(2)-O(2)	1.711	1.710	X(1)-Mo(1)-O(3)	94.10	93.91
Mo(2)-X(2)	2.526	2.771	X(1)-Mo(1)-O(4)	92.11	91.21
Mo(2)-N(3)	2.340	2.306	N(1)-Mo(1)-N(2)	71.05	70.94
Mo(2)-N(4)	2.359	2.313	N(1)-Mo(1)-O(3)	95.97	95.19
Mo(2)-O(4)	1.946	1.946	N(1)-Mo(1)-O(4)	165.02	164.08
Mo(2)-O(3)	1.950	1.950	N(2)-Mo(1)-O(3)	165.32	164.33
			N(2)-Mo(1)-O(4)	96.97	97.11
			O(3)-Mo(1)-O(4)	94.63	95.03
			O(2)-Mo(2)-X(2)	155.28	154.58
			O(2)-Mo(2)-N(3)	83.99	84.89
			O(2)-Mo(2)-N(4)	81.85	82.36
			O(2)-Mo(2)-O(3)	103.45	104.30
			O(2)-Mo(2)-O(4)	103.76	104.42
			X(2)-Mo(2)-N(3)	77.10	75.93
			X(2)-Mo(2)-N(4)	77.19	75.77
			X(2)-Mo(2)-O(3)	91.96	91.21
			X(2)-Mo(2)-O(4)	93.93	93.93
			N(3)-Mo(2)-N(4)	71.61	71.05
			N(3)-Mo(2)-O(3)	165.36	164.07
			N(3)-Mo(2)-O(4)	95.71	95.19
			N(4)-Mo(2)-O(3)	96.69	96.95
			N(4)-Mo(2)-O(4)	164.75	164.31
			O(3)-Mo(2)-O(4)	94.71	95.04

$Mo_2O_4X_2L_2$ (X = Cl, Br) are diamagnetic due to electron pairing via the double bridging oxygen atoms or direct Mo—Mo interaction [57,60].

3.6. Thermogravimetric analysis

Thermogravimetric analyses of complexes **1–4** have been carried out in the temperature range 30°-700 °C with 10 °C/min intervals in N_2 atmosphere to access the structural stability of the complexes (Figs. S3–S6).

The TG-DTA curves of mononuclear complexes $MoOX_3L$ [X = Cl (**1**), Br (**2**)] show one step of mass loss supported by an endothermic peak which corresponds to the loss of the ligand molecule. Complexes **1** and **2** start losing mass at about 380° and 345 °C and show mass loss of 58.65% (Calcd. 57.11%) and 59.33% (Calcd. 57.69%), respectively.

Similarly, TG-DTA curves of binuclear $Mo_2O_4X_2L_2$ complexes [X = Cl (**3**), Br (**4**)] exhibit one step of mass loss supported by an endothermic peak corresponding to the loss of two ligand molecules. At 370°-375 °C temperature range, mass loss of 64.81% (Calcd. 64.03%) and 43.12% (Calcd. 41.68%) occur for complexes **3** and **4**, respectively.

3.7. Electrochemistry

Cyclic voltammograms of the complexes **1–4** were recorded at a Pt-electrode in dry, degassed DMF containing 0.1 M TBAP as supporting electrolyte. The electrochemical data of the complexes are presented in Table 2 and representative cyclic voltammograms for both the mononuclear and binuclear complexes are shown in Fig. 3. The four complexes **1–4** show one irreversible one electron oxidation within the potential range +1.13 to +0.69 V vs SCE [33] which corresponds to Mo(V)/Mo(VI) process. On scan reversal, an irreversible two step one electron reduction peaks are found in the range −0.39 to −0.74 V corresponding to Mo(VI)/Mo(V) couple [61] and −0.74 to −1.54 V for Mo(V)/Mo(IV) couple, respectively.

3.8. DFT calculations: description of the optimized structures of the complexes

The structure of complex **1** was built assuming octahedral geometry around the metal. In addition the ligand could be chelating via (N,N) or (N,S). On considering the free ligand, the conformation with a *cis* N-C-C-N torsion angle of zero proved unstable on DFT optimisation reverting to a *trans* torsion angle providing the conformation for N,S chelation. We therefore considered both types of chelation. For (N,N) chelation there are three possible positions for the terminal oxygen, (a) in an axial position or in an equatorial position *trans* to either (b) N(1) or (c) N(2). The structures of the three possible geometries 1a, 1b and 1c were optimized. 1b and 1c gave the same energy but that of 1a had energy higher by 8.32 kcal/mol. In previous calculations when oxygen atoms were given the 6-31G basis set, structure 1b had a lower energy than 1c by 0.25 kcal/mol and this structure was therefore used in subsequent calculations. A similar set of three structures with the terminal oxygen atom in alternative positions with (N,S) chelation were built, but in each case on optimisation the Mo—S bond was broken so that the Mo…S distance became > 4.0 Å and as a consequence the metal became five-coordinate with a square pyramidal (3Cl, N) environment with the terminal oxygen in an axial position. The energies of all three (N,S) models were > 12 kcal/mol greater in energy than the lowest energy (N,N) chelating model. Structures 1b and 1c had equivalent energies, and the 1b (N,N) model shown in Fig. 4 was chosen at random for further study. For this model, electronic transitions were calculated using the TD-DFT method to compare with the observed peak at 287 nm and seven transitions were found between 315 and 295 nm with f values above 0.035 involving a large number of different orbitals with no specific pattern.

The structure of complex **2** was assumed to be isostructural with complex **1** and also converged successfully (Fig. 4). Dimensions in the coordination spheres are compared in Table 3.

The ligand acts as neutral bidentate N—N donor resembling 2,2′-bipyridine. In complex **1**, the equatorial plane around the molybdenum

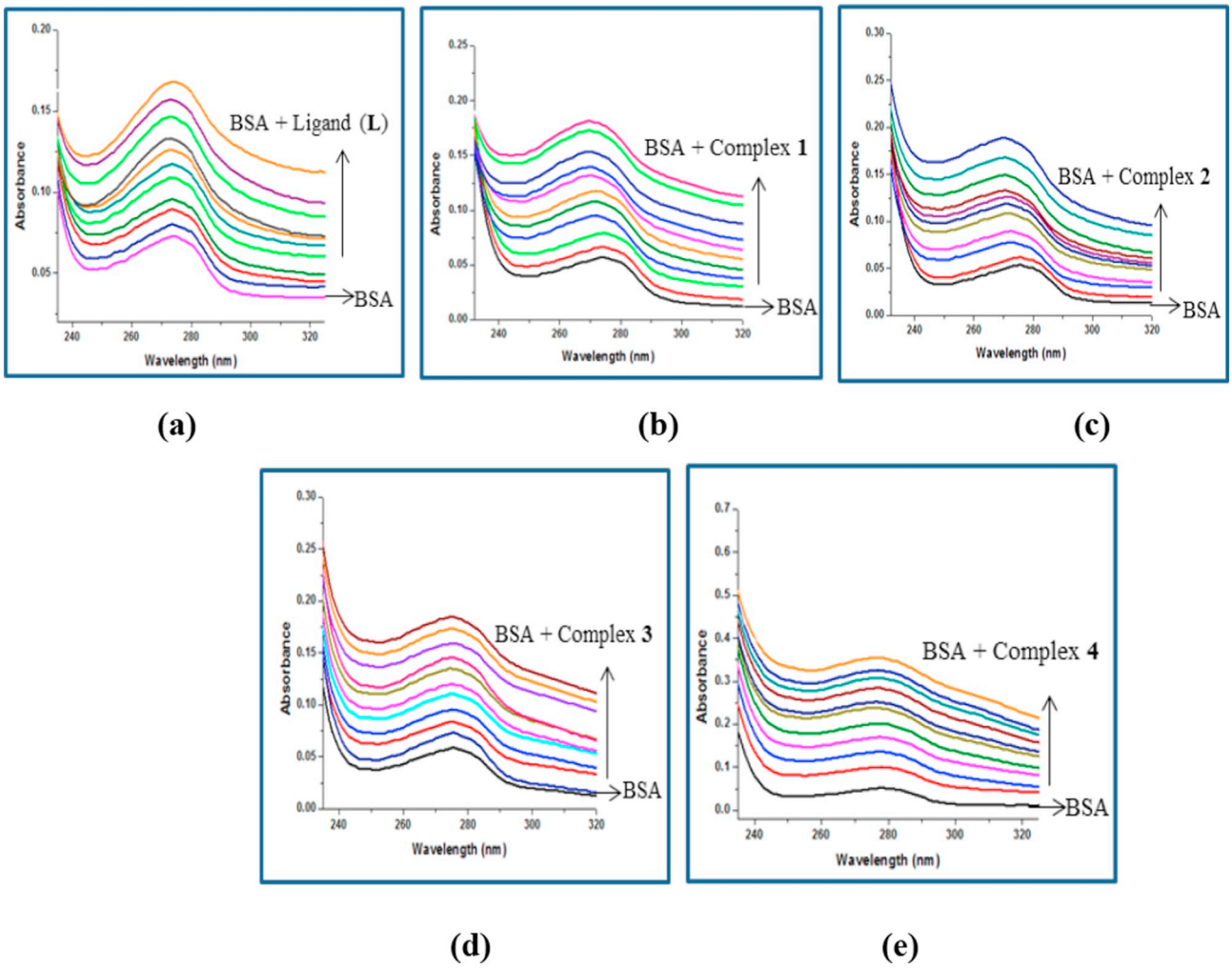

Fig. 6. Absorption spectra of 10^{-5} M BSA with increasing amounts of 10^{-4} M (0–20 μL) (a) ligand (L), (b) complex **1**, (c) complex **2**, (d) complex **3** and (e) complex **4**.

centre can be defined by donor N(2) atom from benzthiazole moiety of the ligand and three chlorine atoms Cl(1), Cl(2), Cl(3) of which Cl(2) and Cl(3) are *trans* to each other with Cl(2)-Mo(1)-Cl(3) bond angle 158.78°. The terminal oxo-oxygen O(1) and donor atom N(1) of the pyrazole moiety occupy the apical positions. The molybdenum atom is displaced by 0.379 Å from the equatorial plane towards the apical oxygen O(1) [33]. The Mo(1)-O(1) bond distance is found to be 1.683 Å [62,63] which is in good agreement with values found in similar oxomolybdenum complexes. A notable difference is observed in Mo—Cl bond distances, the mutually *trans* Mo(1)-Cl(2), Mo(1)-Cl(3) bond distances are 2.4154 Å, 2.401 Å [64] while Mo(1)-Cl(1) distance is only 2.353 Å. The result is compatible with data reported for related molybdenum complexes [65,66]. The Mo(1)-N(2) bond distance is 2.263 Å corresponding to Mo—N single bond distance. The Mo(1)-N(1) bond length extends to 2.455 Å due to the trans influence of the strongly bound terminal oxygen atom. The bite angle N(2)-Mo(1)-N(1) for complex **1** is 68.89° [33]. The axial-Mo(1)-equatorial bond angles deviate from the 90^0 which is expected for idealized octahedral geometry and this is presumably due to the relatively small bite angle in the complex. As is apparent from Table 3, complex **2** has a similar coordination environment to that of complex **1**.

For complexes **3** and **4**, the dimer containing a Mo_2O_2 core, with X = Cl and Br respectively, there are two possible structures with the two terminal oxygen atoms either *cis* or *trans*. It was apparent however that the *trans* structure was most unlikely due to the close contacts between the phenyl rings. The *cis* structure was refined successfully with paired electrons and the resulting structure of **3** with X = Cl is shown in Fig. 5. Dimensions are shown in Table 4. There is clearly a bond between the two metal atoms at a distance of 2.597 Å. This distance is comparable to that found in similar dimeric structures of Mo(V) [67] where distances of 2.620(1) Å, 2.608(1) Å are found which validates the DFT methodology used in this work. The structure was then optimized with two unpaired electrons and converged successfully with an energy higher by 11.68 kcal/mol and Mo···Mo distance of 2.981 Å.

The structure of **4** was built from the optimized structure of **3** but with Cl replaced by Br and converged to a similar structure with a Mo···Mo distance of 2.580 Å. Apart from the Mo—Br distances, the remaining dimensions in **4** are very similar to those in **3** as shown in Table 4.

Binuclear complex **3** possesses a $[Mo_2O_4]^{2+}$ core having a twofold axis of symmetry. The two terminal oxygen atoms O(1) and O(2) are mutually *cis*. The two bridging oxygen atoms O(3), O(4) and four donor N sites from two coordinated ligands occupy the equatorial plane while the chlorine atoms are *trans* to each terminal O(1) and O(2). The Mo(1)-O(1) and Mo(2)-O(2) bond distances are equivalent at 1.708, 1.711 Å [48] while the *trans* Mo(1)-Cl(1) and Mo(2)-Cl(2) distances are lengthened at 2.523, 2.526 Å due to the *trans* influence of the terminal oxygen atoms. The four Mo—O bond lengths involving the bridging oxygen atoms are in the range 1.946–1.950 Å which are comparable to those in other dioxo bridged Mo(V) structures [52]. The Mo—Mo distance of 2.597 Å corresponds to a single bond length between two molybdenum atoms [68]. The Mo(1)-N(1), Mo(2)-N(3) bond distances at 2.336, 2.340 Å are slightly shorter than the Mo(1)-N(2) and Mo(2)-N(4) bonds at 2.354, 2.359 Å. The molybdenum atoms are displaced from

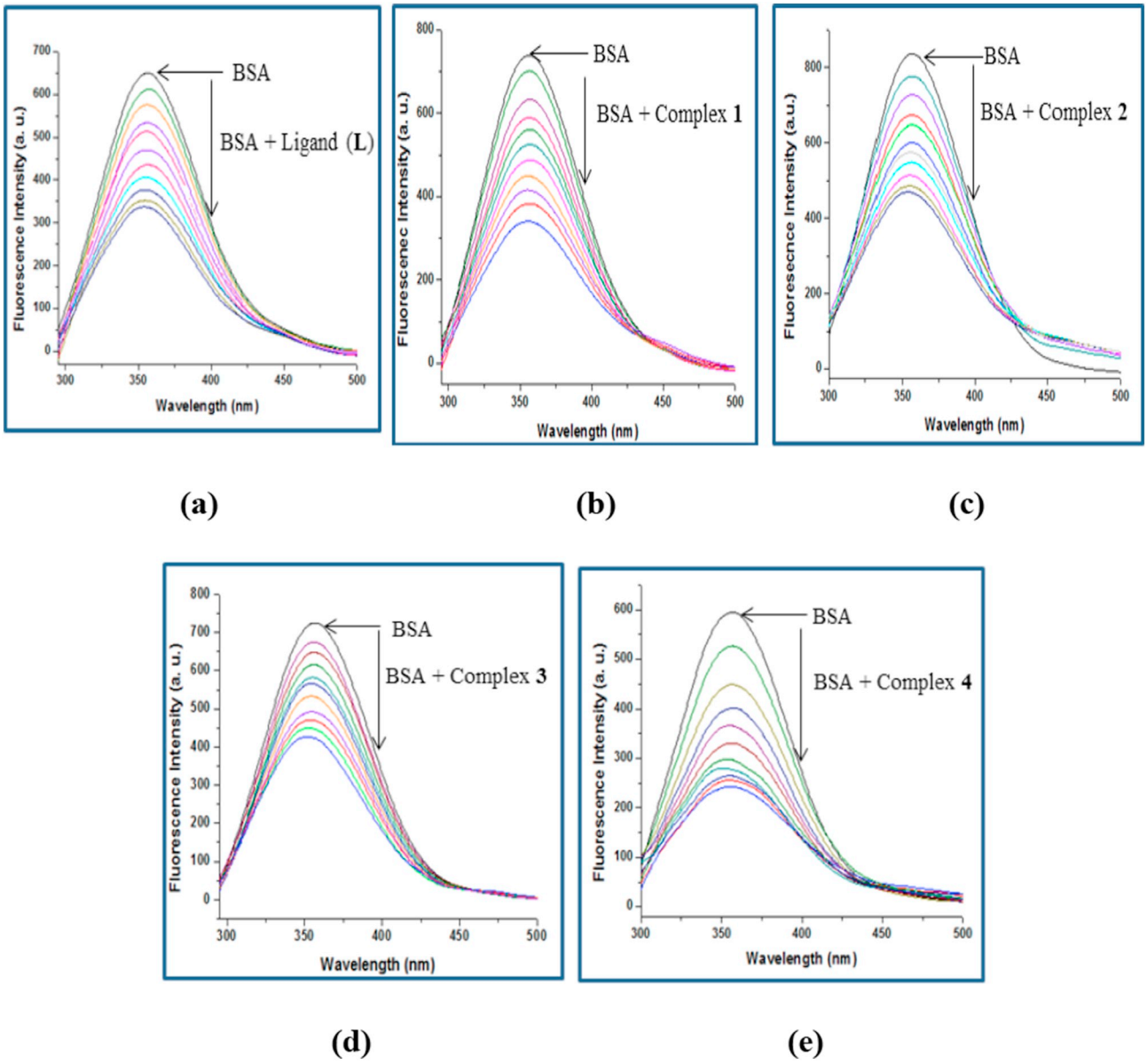

Fig. 7. Fluorescence quenching spectra of 10^{-5} M BSA with increasing amounts of 10^{-4} M (0–20 μL) (a) ligand (L), (b) complex **1**, (c) complex **2**, (d) complex **3** and (e) complex **4**.

the median plane by 0.173 Å and 0.174 Å at the two centres. Complex **4** has a similar coordination environment to that of complex **3**.

Using the optimized structures, the frontier orbitals of the complexes were calculated and representative diagrams are shown in Figs. S7–S8.

Electronic transitions for **3** were calculated using the DFT-TD method with dichloromethane as the solvent. The most intense electronic transition is to be found at 490.9 nm which agrees well with the experimental value of 491 nm. This agreement confirms that the postulated dimeric structure of complex **3** with a Mo—Mo bond is correct. This transition is from the HOMO to LUMO + 1. As shown in Fig. S8, the major contributions to the HOMO are from the central MO_2O_2 moiety, using the Mo 7d + 2 orbitals of Mo and the 2py, 3py orbitals of the oxygen atoms and while only ligand atoms contribute to LUMO + 1.

3.9. Interaction with BSA protein

3.9.1. Absorption titration studies

To investigate the interaction of the ligand (L) and complexes **1**–**4** with BSA protein, UV–Vis absorption titration studies were performed in aqueous solution at pH = 7 (phosphate buffer) at room temperature. Initially, BSA showed its absorption peak at 275 nm, then the absorption spectra of BSA was recorded at different concentrations (0–20 μL) of the compounds. From the spectra (Fig. 6), it has been found that the absorbance of BSA increased remarkably with incremental addition of the compounds accompanied with hypsochromic shifts of ~2–3 nm. The gradual enhancement of absorbance of BSA indicates association between the compounds and BSA to form a non-fluorescent ground-state complex. Thus, static mode of quenching of the fluorophore is predicted.

3.9.2. Fluorescence titration studies

Small molecules and serum protein interaction are significant characteristics of metal drug metabolism and can possibly affect the biotransformation and the mechanism of the chemotherapeutic agents [69]. Fluorescence spectroscopy is most often used to study the interaction of small molecules with BSA. In the protein binding studies, BSA is usually preferred over other proteins due to its abundance, low cost,

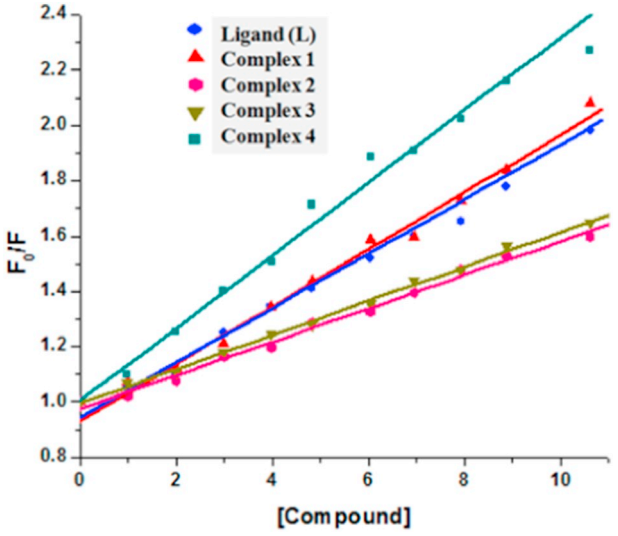

Fig. 8. Stern-Volmer plots of the fluorescence titration of the ligand and the complexes with BSA.

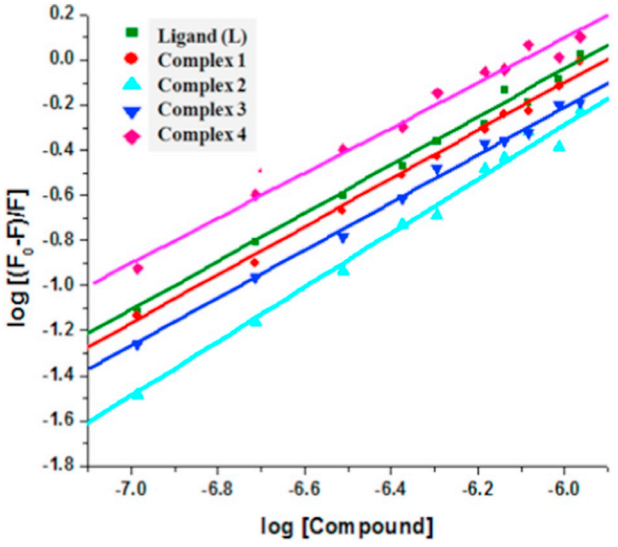

Fig. 9. Plot of log $[(F_0-F)/F]$ vs. log [Q] for the fluorescence titration of the ligand and the complexes with BSA.

Table 5
Stern-Volmer constant (K_{SV}), protein binding constant (K_b) and number of binding sites (n) of the ligand (L) and complexes **1–4**.

Compounds	K_{SV} (M^{-1})	K_b (M^{-1})	n
Ligand (L)	0.985×10^6	2.269×10^6	1.06
Complex **1**	1.034×10^6	2.004×10^6	1.06
Complex **2**	0.604×10^6	1.987×10^6	1.08
Complex **3**	0.617×10^6	1.436×10^6	1.06
Complex **4**	1.313×10^6	1.258×10^6	1.00

stability and due to its similarity with human serum albumins (HSA) [70]. BSA consists of three fluorophores tryptophan (Trp), tyrosine (Tyr) and phenylalanine (Phe) of which tryptophan (Trp) is primarily responsible for the intrinsic fluorescence of BSA [71]. Here we have studied the binding interaction of BSA with the ligand and the four oxomolybdenum(V) complexes **1–4** qualitatively with the help of fluorescence spectroscopy. In the present investigation, fluorescence emission spectra of BSA are recorded in the absence and presence of the compounds (quenchers). In the absence of quenchers, BSA gives a strong emission band at 356 nm upon excitation at 275 nm. The intrinsic tryptophan fluorescence intensity of BSA was found to quench progressively in a consistent manner on gradually increasing the quencher concentration (0–20 μL) accompanied with hypsochromic shifts of 2.5, 1.5, 2.5, 1.5 and 1.5 nm for the ligand and the complexes **1**, **2**, **3** and **4** respectively. The concentration dependent quenching of protein fluorescence intensity by the ligand and the complexes is shown in Fig. 7. The observed quenching of the fluorescence intensity and blue shift of the wavelength of BSA can be attributed to the perturbation of the conformation of the protein due to binding interactions between the complexes and BSA which lead to changes in the fluorophore environment [72–75]. Tryptophan, the active site of the protein, gets buried into the hydrophobic environment containing amino acids leucine, tyrosine and phenylalanine (protein refolding). This leads to changes in polarity which are indicated by the hypsochromic shifts.

It is also observed that at higher quencher concentration, the fluorescence intensity ultimately reaches a constant minimum value which indicates the protein saturation point. The constant intensity attained may be predicted as being due to the presence of the free ligand and complexes. Changes in the emission spectrum do not occur beyond the protein saturation point, since no further alteration occurs in the fluorophore microenvironment.

In order to understand quantitatively the magnitude of interaction between the compounds and BSA, data were analyzed using the Stern-Volmer equation [76]:

$$F_0/F = 1 + K_{SV}[Q]$$

where, F and F_0 are the fluorescence intensities, with and without quencher respectively, K_{SV} is the Stern-Volmer constant and [Q] is the concentration of the quencher. K_{SV} was obtained from the slope of F_0/F versus [Q] plot (Fig. 8). Values of K_{SV} for the ligand and the complexes **1–4** are found to be in the order of 10^6 which indicate their high quenching abilities. The nature of F_0/F versus [Q] curves is linear indicating static quenching mechanism, i.e. formation of fluorophore-quencher adducts in the ground state.

In protein binding studies, the binding constant (K_b) and the number of binding sites per albumin (n) are given by the following equation [72]:

$$\log[(F_0 - F)/F] = \log K_b + n \log[Q]$$

From the plot of log $[(F_0-F)/F]$ versus log [Q] (Fig. 9), n was obtained from the slope and K_b was obtained from the intercept. Values of K_{SV}, K_b and n for the interaction of the ligand and the complexes are shown in Table 5. K_b values were found to be sufficiently high to confirm reversible binding and release of the compounds from BSA. Close examination of the K_b values reveals an interesting phenomenon. The mononuclear complexes being smaller in size than the binuclear complexes have a slightly stronger interaction with BSA. Thus, a noticeable correlation between the complex size and BSA binding ability is found. At experimental temperature, the n values for all the complexes are approximately equal to unity which indicates the availability of only one binding site per albumin.

3.10. Evaluation of in vitro cytotoxicity of the ligand and complexes

3.10.1. Effects on cell death

To establish the optimum cytotoxic effect of the ligand (L) and oxomolybdenum(V) complexes **1–4**, MTT cell viability assays were carried out. The cytotoxicity assay is the most basic study to determine the anticancer ability of any compound. The toxic effects were found to be specific for each compound and type of cell and dependent upon incubation time and concentration. Out of the five compounds tested for their toxicity on three different cell lines [human cervix adenocarcinoma epithelial cells (HeLa), human renal cell carcinoma (SK-RC-45) and human breast adenocarcinoma cells (MCF-7)], the ligand did not show significant toxicity compared to the oxomolybdenum(V)

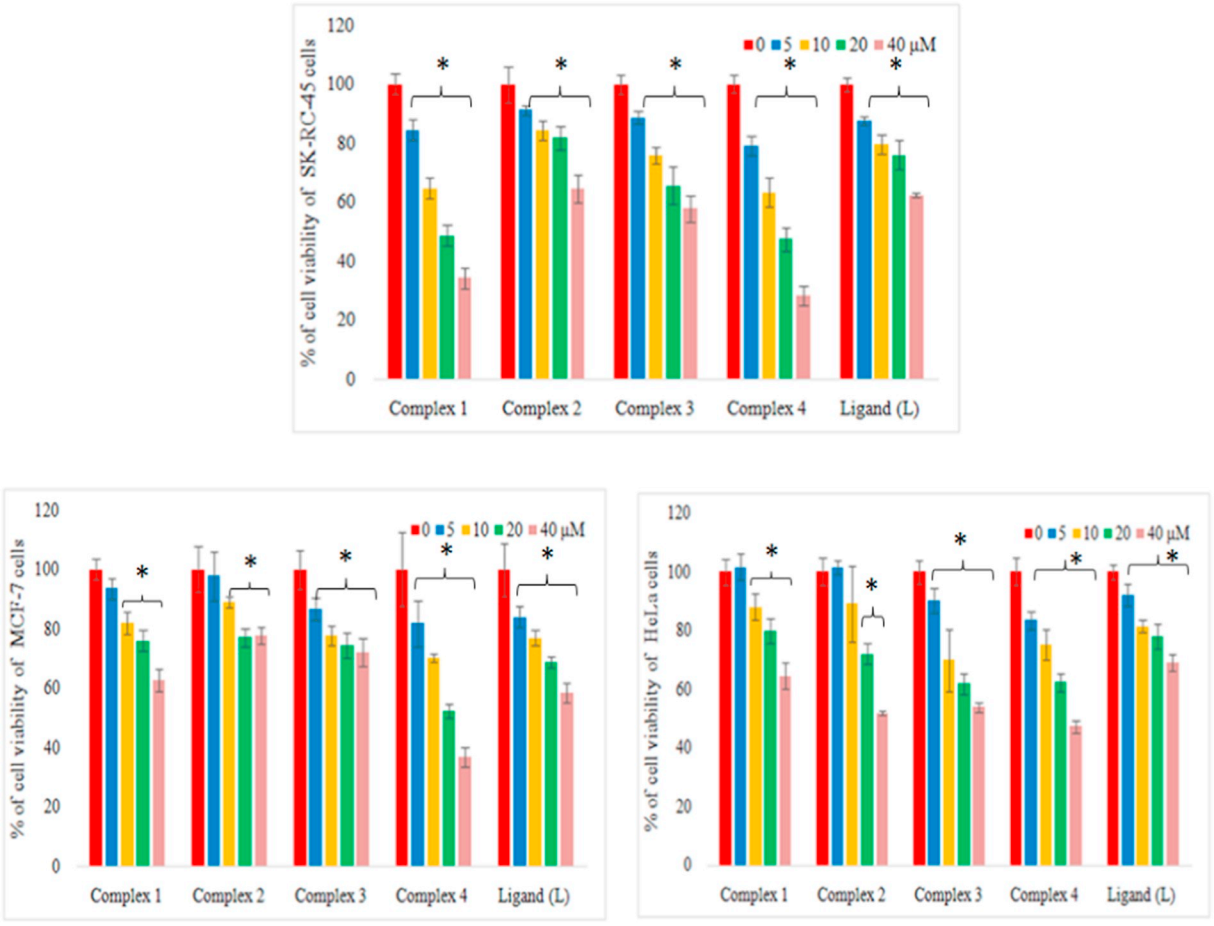

(a)

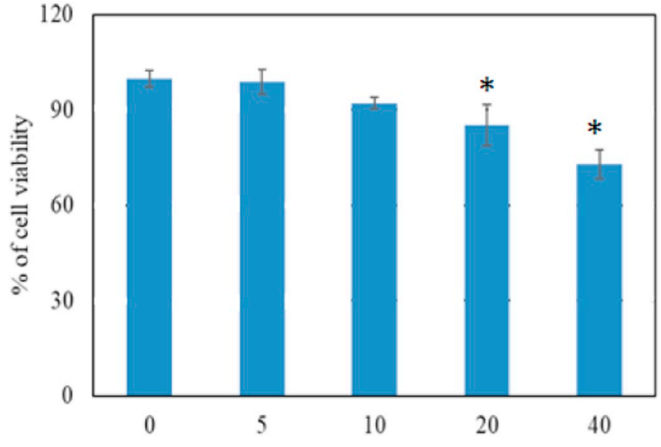

(b)

Fig. 10. (a) Dose dependent cytotoxic efficacy of the ligand (L) and oxomolybdenum(V) complexes **1**–**4**. (b) Dose dependent cytotoxic efficacy of complex **4** on NKE cells. The cytotoxic efficacy of the compounds is expressed in percentage of the control value. The untreated cells were considered as control."*" represents the significant difference between the normal control and treated cells ($P^* < 0.05$).

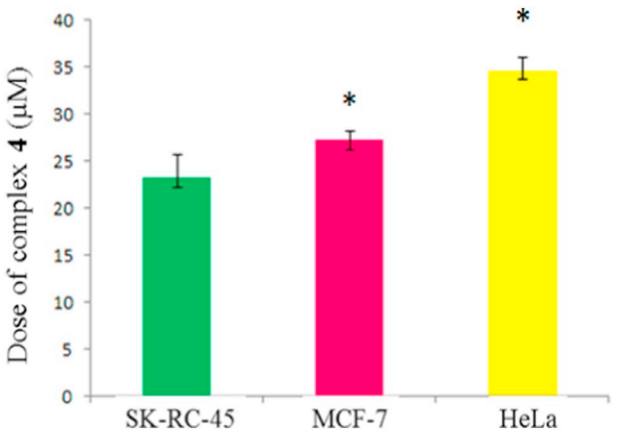

Fig. 11. LC_{50} values of complex **4** in different cell lines. "*" represents the significant difference between the normal and treated cells ($P^* < 0.05$).

complexes. The SK-RC-45 cell line was most sensitive to all the compounds compared to the other two cell lines (HeLa and MCF-7) (Fig. 10). Complex **4** exhibited maximum cytotoxicity compared to the other complexes in all types of cancer cells. Complex **4** reduced cell viability by 27% at 40 μM dose which was significantly less than the toxicity showed in SK-RC 45 cells. The LC_{50} values for complex **4** have been calculated from the cell viability graph (Fig. 11). The LC_{50} values of the molybdenum complexes on three cell lines indicate that these complexes may act differently on the cell lines. The correlation between

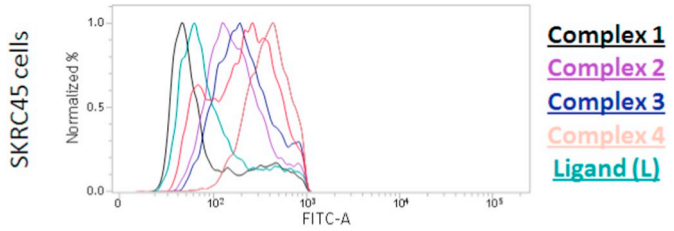

Fig. 13. FACS analysis with H_2DCFDA in the SK-RC-45. The cells were exposed to 40 μM of each compound. The x-axis in the figures represents the fluorescence intensity of the DCFDA.

the structures of the synthesized compounds and their anticancer activities leads to the conclusion that the complexes bearing bromine atoms possess higher potencies in MTT assay.

The mode of cell death may be apoptotic or necrotic. In order to confirm these results and determine the mode of cytotoxicity, FACS analysis was performed with all the compounds. In line with the results of MTT cell viability experiments, it was observed that at a dose of 40 μM, complex **4** is the most effective compound in inducing cytotoxicity in all the three types of cancer cells. Interestingly, it was observed that the cytotoxicity was induced following apoptotic pathway since, annexin V staining facilitates the detection of apoptotic cells by binding to the phosphatidyl serine moiety in the outer surface of the plasma membrane (Figs. 12, S9). Apoptosis is a biochemical event that leads to cell death. It can be characterized by changes in cellular morphology, plasma membrane blebbing, chromatin condensation, DNA fragmentation and many more.

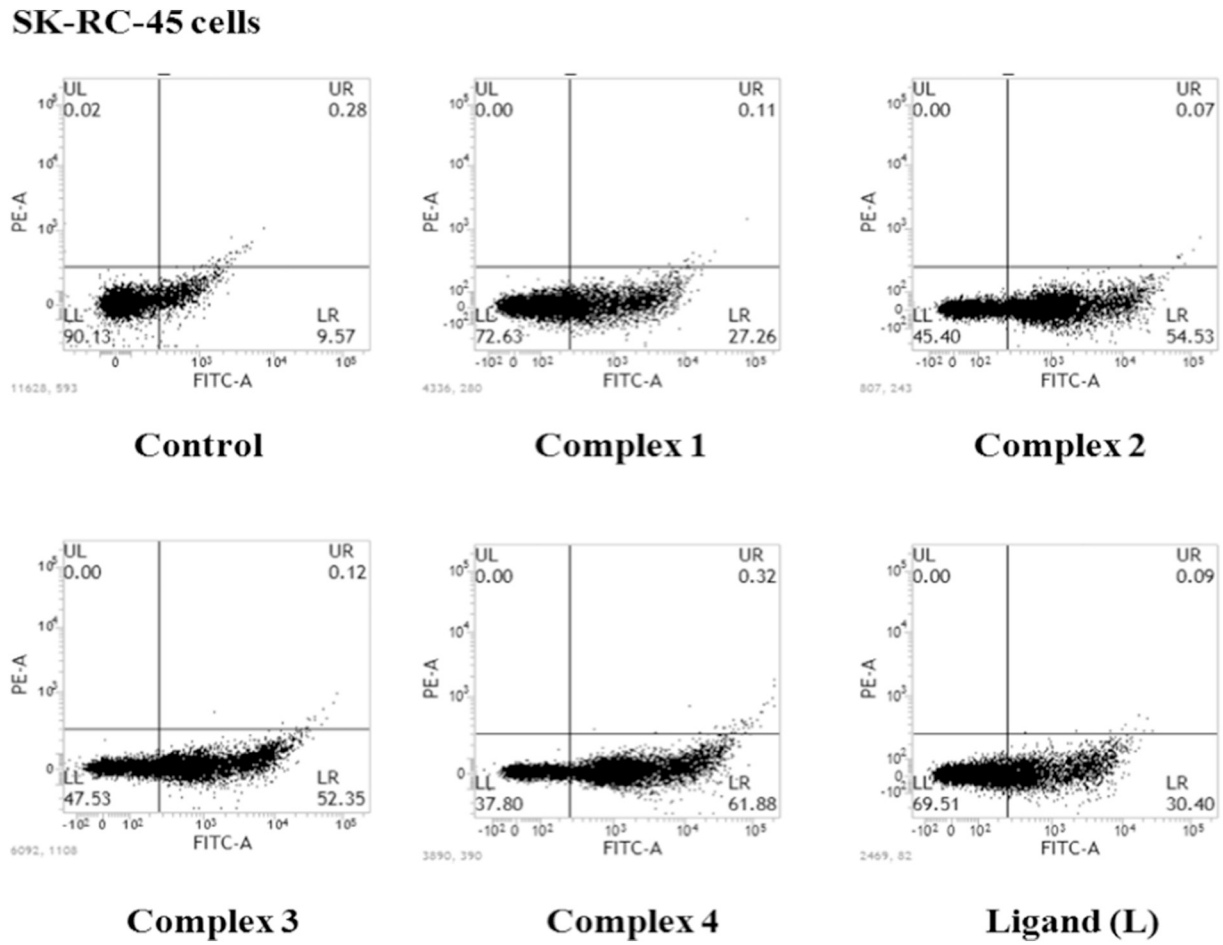

Fig. 12. FACS analysis with annexin V-FITC in the SK-RC-45 cell. The cells were exposed to 40 μM of each compound. The lower left quadrant represents the untagged cells (non-apoptotic cells) and the cells in the lower right quadrant represent the FITC tagged cells (apoptotic cells).

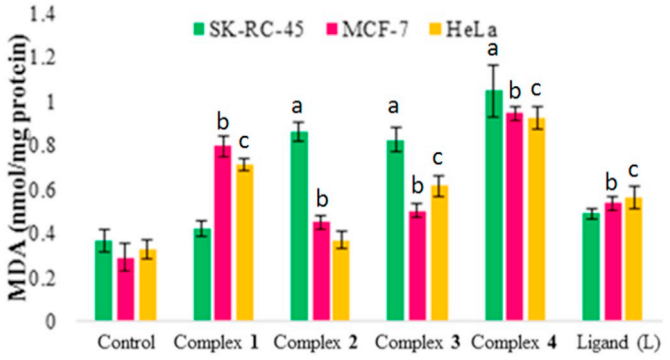

Fig. 14. Quantification of lipid peroxidation in the SK-RC-45, MCF-7 and HeLa cells. The cells were exposed to 40 μM of each compound. "a" "b" and "c" represents the significant difference between the control and treated cells ($P^* < 0.05$).

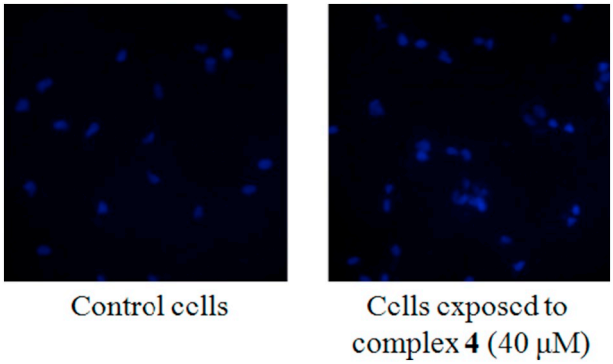

Fig. 16. Fluorescent micrographs of DAPI stained SK-RC-45 cells exposed to 40 μM of complex **4** for 24 h. The imaging was done at 20× magnification.

3.10.2. Effects on oxidative stress

All the molybdenum complexes **1–4**, but not ligand (L), were found to significantly elevate the level of intracellular ROS in the cancer cells at a dose of 40 μM. Complex **4** is found to be the most effective in inducing significant oxidative stress in all the cancer cells, particularly in the SK-RC-45 cells. The induction of oxidative stress in the cancer cells can be correlated with the induction of cell death, since the cancer cells are more vulnerable to exogenous ROS insult (Figs. 13, S10) [47].

3.10.3. Effects on lipid peroxidation

The molybdenum complexes **1–4** were found to induce lipid peroxidation in the cancer cells although the ligand itself did not show any significant effect. Among the four complexes, complex **4** was found to be the most effective in this regard at a dose of 40 μM (Fig. 14). Lipid peroxidation indicates the oxidative degradation of intracellular lipids due to the accumulation of free radicals. Therefore, detection of lipid peroxidation indicates the occurrence of oxidative stress.

The experimental results on cell death, oxidative stress and lipid peroxidation of the SK-RC-45 cells suggest complex **4** to be the most active. These encouraging results with complex **4** on the SK-RC-45 cell line led us to deepen our investigation. The effect of complex **4** was further studied on the cellular morphology, DNA fragmentation and colony formation ability against the SK-RC-45 cell line.

3.10.4. Effects on cellular morphology

Exposure of 40 μM of complex **4** to the SK-RC-45 cells causes significant alterations in cellular morphology compared to the control cells. Micrographs showed that complex **4** causes time dependent cytotoxicity to the renal cancer cells at this concentration. Severe morphological changes (such as membrane blebbing, increased spherical shaped cells and apoptotic bodies) were observed in the micrographs observed at 18 h and 24 h. The number of cells with membrane blebbing and apoptotic cells increased with time in complex **4** treated SK-RC-45 cell plates (Fig. 15).

3.10.5. Effects on DNA fragmentation

To confirm the induction of apoptosis in the SK-RC-45 cells due to the exposure of 40 μM of complex **4**, microscopic experiments were performed with DAPI. Since DAPI is a DNA binding dye, it gives bright blue fluorescence when the cellular DNA or the nuclear morphology is intact. On the onset of apoptosis cellular DNA gets fragmented and the nuclear morphology gets perturbed. After 24 h exposure of 40 μM of

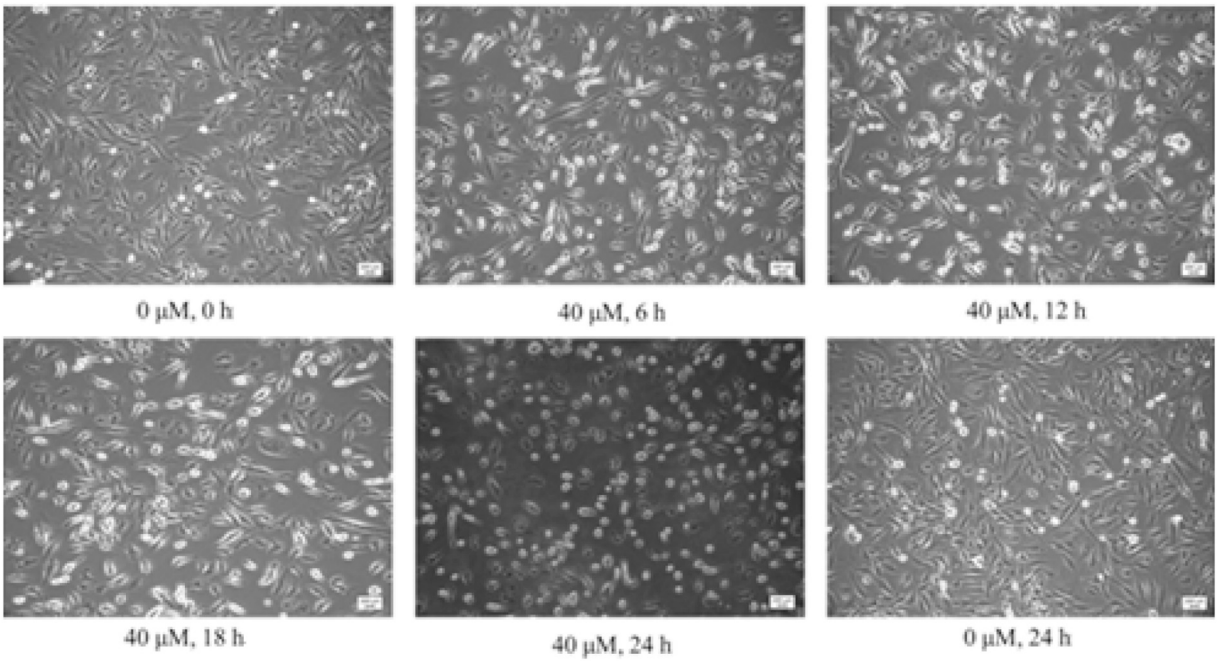

Fig. 15. Phase contrast micrographs of SK-RC-45 cells exposed to 40 μM of complex **4**. The imaging was done at an interval of 6 h for a total time period of 24 h. The cells were observed under 10× magnification.

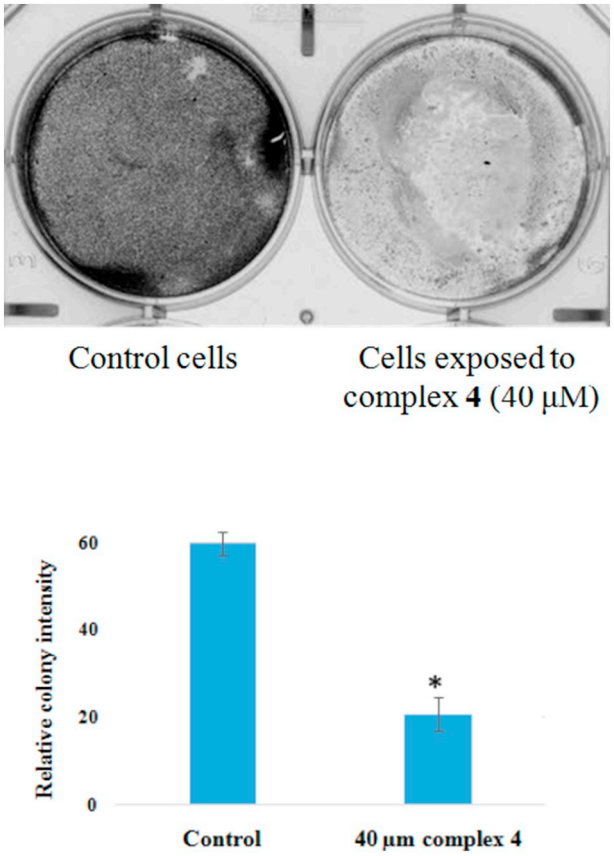

Fig. 17. Effect of complex **4** (40 μM) on colony forming ability of SK-RC-45 cells post exposure.

complex **4**, the nuclear morphology appears to be perturbed under fluorescent microscope at 20× magnification compared to the normal cells, where the nucleus appears significantly intact with a bright blue DAPI fluorescence (Fig. 16).

3.10.6. Effects on colony formation ability

To investigate the anticancer potential of complex **4** (the most effective compound), a colony forming assay was performed with the SK-RC-45 cells. Complex **4** (40 μM) showed significant inhibition in the colony formation in the renal cancer cells (Fig. 17).

The above results clearly indicate that the nature of the halogen atom plays a key role in anticancer activity. The presence of bromine atoms in complexes **2** and **4** intensified the cytotoxic levels compared to complexes **1** and **3** containing chlorine atoms. Hence, the electronic characteristics of the halogen atoms bound to molybdenum have a direct influence on the ability of the complexes to interact with the biological target. Complex **4** was found to be the most potent member of the series against the SK-RC-45 cell line. Thus, the bromine atoms indeed augment the cytotoxicity of the complex.

It may be predicted from the literature that as a result of binding of the complexes with DNA, the replication and transcription of DNA is inhibited [77,78]. Progressive sequential release of the halide ligands may typically occur as in the case of cisplatin [79]. Moreover, it can be concluded that induction of oxidative stress can be a possible reason behind the cytotoxic activity of the newly synthesized molybdenum compounds.

The reason for the better performances by complexes **2** and **4** might be partially explained by the greater lipophilicity of the bromo analogues compared to their chloride counterparts. Greater lipophilicity ensures an enhanced cellular uptake of complexes **2** and **4**. The greater activity of the bromo analogues can also be due to the difference in the kinetics of halide release during their interactions with DNA. Hence, switching over from the chloride to bromide could offer an effective therapeutic advantage.

From these studies an overall chemical and biological profile emerges for $MoOX_3L$ [X = Cl (**1**), Br (**2**)] and $Mo_2O_4X_2L_2$ [X = Cl (**3**), Br (**4**)] complexes. The slight but meaningful differences observed between the chloro and bromo complexes might be advantageously exploited for future clinical applications. Thus, our study provides new useful insights for designing molybdenum containing drugs for anticancer therapy.

4. Conclusions

Four new oxomolybdenum(V) complexes **1–4** have been synthesized and characterized with the aim of evaluating their anticancer properties. The spectroscopic (IR, electronic, EPR), magnetic and electrochemical investigations of the complexes reveal the coordination environment and oxidation state of the metal centre in the complexes. The molecular structures of the complexes were established with the help of DFT calculations. The complexes were found to be thermally stable up to ~350 °C. Absorption and fluorescence titrations reveal that the ligand and complexes bind with BSA protein. The number of binding sites (n) is approximately equal to unity which indicates the availability of only one binding site per albumin.

Molybdenum complexes differing only in the chemical nature of the halide ligands were studied. Very interesting chemical and biological features of the compounds emerged. Cellular studies were performed on three different human cancer cell lines. The activity of the free ligand was found to be negligible against all the cell lines. Notably, the bromo analogue turned out to have strong cytotoxic effects on different cancer cell lines in vitro. Specifically, complex **4** showed prominent results against the SK-RC-45 cell line. The bromine atoms in complex **4** act as uptake shuttle and efficacy booster. Hence, the results obtained confirm the significance and importance of the anticancer study.

Abbreviations

IR	infrared
UV–Vis	ultraviolet-visible
EPR	electron paramagnetic resonance
DFT	density functional theory
BSA	bovine serum albumin
HeLa	cervix adenocarcinoma epithelial cells
SK-RC-45	renal carcinoma cells
MCF-7	breast adenocarcinoma cells
NKE	human normal kidney epithelial cells
SA	serum albumin
HSA	human serum albumin
TBAP	tetra butyl ammonium perchlorate
DMEM	Dulbecco's modified eagle medium
FBS	fetal bovine serum
PBS	phosphate buffered saline
MTT	3-(4,5-dimethylthiazol-2-yl)-2,5-diphenyltetrazolium bromide
FITC	fluorescein isothiocyanate
FACS	fluorescence assisted cell sorting
ROS	reactive oxygen species
H_2DCFDA	2′,7′-dichlorodihydrofluorescein diacetate
MDA	malondialdehyde
DAPI	4′,6-diamidino-2-phenylindole
TG-DTA	thermogravimetry-differential thermal analysis
TD-DFT	time dependent density functional theory
HOMO	highest occupied molecular orbital
LUMO	lowest unoccupied molecular orbital

Acknowledgements

M. Roy acknowledges UGC for the Junior Research Fellowship. D. Biswal acknowledges UGC for the Senior Research Fellowship. The authors thank Prof. Pramit Chowdhury (IIT Delhi) for thermal analysis. We would also like to thank the reviewers for giving such valuable and constructive suggestions which led to the improvement of quality of this article.

Appendix A. Supplementary data

Supplementary Figs. S1, S2, S3–S6 and S7–S8 contain the IR spectra of the ligand, complex **1** and complex **4**, ESI-MS of ligand and the complex **2**, TG-DT curves of complexes **1–4** and the frontier orbitals in complexes **1** and **3**, respectively. Fig. S9 shows the FACS analysis with annexin V-FITC in the MCF-7 and HeLa cells. Fig. S10 shows FACS analysis with H_2DCFDA in the MCF-7 and HeLa cells. Supplementary data to this article can be found online at https://doi.org/10.1016/j.jinorgbio.2019.110755.

References

[1] V. Vrdoljak, D. Milić, M. Cindrić, D.M. Čalogović, J. Pisk, M. Marković, P. Novak, Z. Anorg. Allg. Chem. 635 (2009) 1242.
[2] I. Sheikhshoaie, A. Rezaeifard, N. Monadi, S. Kaafi, Polyhedron 28 (2009) 733.
[3] A. Rezaeifard, I. Sheikhshoaie, N. Monadi, M. Alipour, Polyhedron 29 (2010) 2703.
[4] S. Pasayat, S.P. Dash, P.K. Majhi, Y.P. Patil, M. Nethaji, H.R. Dash, S. Das, R. Dinda, Polyhedron 38 (2012) 198.
[5] R.D. Chakravarthy, K. Suresh, V. Ramkumar, D.K. Chand, Inorg. Chim. Acta 376 (2011) 57.
[6] A. Capapé, M.D. Zhou, S.L. Zang, F.E. Kühn, J. Organomet. Chem. 693 (2008) 3240.
[7] C.D. Brondino, M.J. Romão, I. Moura, J.J. Moura, Curr. Opin. Chem. Biol. 10 (2006) 109.
[8] H.K. Saha, M.C. Halder, J. Inorg. Nucl. Chem. 33 (1971) 3719.
[9] H.K. Saha, A.K. Banerjee, J. Inorg. Nucl. Chem. 34 (1972) 697.
[10] H.K. Saha, S. Chakraborti, M. Bagchi, J. Inorg. Nucl. Chem. 36 (1974) 455.
[11] H.K. Saha, A.K. Banerjee, Inorg. Synth. 15 (1974) 100.
[12] H.K. Saha, S.S. Mandal, J. Inorg. Nucl. Chem. 38 (1976) 1868.
[13] H.K. Saha, A.K. Saha, S.S. Mandal, J. Indian Chem. Soc. 12 (1985) 704.
[14] S.S. Mandal, P.C. Ghorai, N.R. Pramanik, T.K. Raychaudhuri, J. Indian Chem. Soc. 74 (1997) 212.
[15] M. Frezza, S. Hindo, D. Chen, A. Davenport, S. Schmitt, D. Tomco, Q.P. Dou, Curr. Pharm. Des. 16 (2010) 1813.
[16] K.D. Mjos, C. Orvig, Chem. Rev. 114 (2014) 4540.
[17] M.P. Coughlan, J. Inherit. Metab. Dis. 6 (1983) 70.
[18] G.A. Hampannavar, R. Karpoormath, M.B. Palkar, M.S. Shaikh, B. Chandrasekaran, ACS Med. Chem. Lett. 7 (2016) 686.
[19] R.K. Gill, R.K. Rawal, J. Bariwal, Arch. Pharm. 348 (2015) 155.
[20] S.S. Bhatt, B.R. Saha, P.B. Trivedi, N.K. Undavia, N.C. Desai, Indian J. Chem. Sect. B 33 (1994) 189.
[21] R.S. Lodhi, S.D. Srivastava, S.K. Srivastava, Indian J. Chem. Sect. B 37 (1998) 899.
[22] B.D. Naik, K.R. Desai, Asian J. Chem. 16 (2004) 1749.
[23] R. Yadav, S. Srivastava, S.K. Srivastava, S.D. Srivastava, Chem. Indian J. 1 (2003) 95.
[24] S.T. Huang, I.J. Hsei, C. Chen, Bioorg. Med. Chem. 14 (2006) 6106.
[25] M. Singh, S.K. Singh, M. Gangwar, G. Nath, S.K. Singh, RSC Adv. 4 (2014) 19013.
[26] T. Akhtar, S. Hameed, N. Al-Masoudi, R. Loddo, P. Colla, Acta Pharma. 58 (2008) 135.
[27] K.N. Venugopala, M. Krishnappa, S.K. Nayak, B.K. Subrahmanya, J.P. Vaderapura, R.K. Chalannavar, R.M. Gleiser, B. Odhav, Eur. J. Med. Chem. 65 (2013) 295.
[28] N. Siddiqui, M. Alam, A.A. Siddiqui, Asian J. Chem. 16 (2004) 1005.
[29] B.M. Gurupadayya, M. Gopal, B. Padmashali, V.P. Vaidya, Ind. J. Heterocy Chem. 15 (2005) 169.
[30] S. R. Pattan, Ch Suresh, V. D. Pujar, V. V.K. Reddy, V.P. Rasal, B.C. Koti, Ind. J. Chem. 44B (2005) 2404.
[31] S.P. Singh, S. Segal, Ind. J. Chem. 27B (1988) 941.
[32] P.U. Maheswari, M. van der Ster, S. Smulders, S. Barends, G.P. van Wezel, C. Massera, S. Roy, H. den Dulk, P. Gamez, J. Reedijk, Inorg. Chem. 47 (2008) 3719.
[33] N.R. Pramanik, S. Ghosh, T.K. Raychoudhuri, M.G.B. Drew, T.K. Mandal, S.S. Mandal, Inorg. Chim. Acta 383 (2012) 60.
[34] G. Coni, M. Massacesi, G. Ponticelli, G. Puggioni, C. Putzolu, Transit. Met. Chem. 12 (1987) 379.
[35] S. Sengupta, J. Gangopadhyay, A. Chakravorty, Dalton Trans. (2003) 4635.
[36] G.M. Nitulescu, C. Draghici, O.T. Olaru, Int. J. Mol. Sci. 14 (2013) 21805.
[37] J. Sun, Y. Zhou, Molecules 20 (2015) 4383.
[38] Y. Li, H.Q. Zhang, J. Liu, X.P. Yang, Z.J. Liu, J. Agric. Food Chem. 54 (2006) 3636.
[39] H. Song, Y. Liu, L. Xiong, Y. Li, N. Yang, Q. Yang, J. Agric. Food Chem. 60 (2012) 1470.
[40] F. Mani, C. Mealli, Inorg. Chim. Acta 63 (1982) 97.
[41] K. Hirayama, S. Akashi, M. Furuya, K. Fukuhara, Biochem. Biophys. Res. Commun. 173 (1990) 639.
[42] M. J. Frisch, G. W. Trucks, H. B. Schlegel, G. E. Scuseria, M. A. Robb, J. R. Cheeseman, J. A. Montgomery, T. Vreven, K. N. Kudin, J. C. Burant, J. M. Millam, S. S. Iyengar, J. Tomasi, V. Barone, B. Mennucci, M. Cossi, G. Scalmani, N. Rega, G. A. Petersson, H. Nakatsuji, M. Hada, M. Ehara, K. Toyota, R. Fukuda, J. Hasegawa, M. Ishida, T. Nakajima, Y. Honda, O. Kitao, H. Nakai, M. Klene, X. Li, J. E. Knox, H. P. Hratchian, J. B. Cross, V. Bakken, C. Adamo, J. Jaramillo, R. Gomperts, R. E. Stratmann, O. Yazyev, A. J. Austin, R. Cammi, C. Pomelli, J.W. Ochterski, P. Y. Ayala, K. Morokuma, G. A. Voth, P. Salvador, J. J. Dannenberg, V. G. Zakrzewski, S. Dapprich, A. D. Daniels, M. C. Strain, O. Farkas, D. K. Malick, A. D. Rabuck, K. Raghavachari, J. B. Foresman, J. V. Ortiz, Q. Cui, A. G. Baboul, S. Clifford, J. Cioslowski, B. B. Stefanov, G. Liu, A. Liashenko, P. Piskorz, I. Komaromi, R. L. Martin, D. J. Fox, T. Keith, M. A. Al-Laham, C. Y. Peng, A. Nanayakkara, M. Challacombe, P. M. W. Gill, B. Johnson, W. Chen, M. W. Wong, C. Gonzalez, J. A. Pople, Gaussian 03, Revision C.02; Gaussian, Inc.: Wallingford. CT, U.S.A. 2004.
[43] S. Saha, P. Sadhukhan, K. Sinha, N. Agarwal, P.C. Sil, Biochemistry and biophysics reports 5 (2016) 313.
[44] S. Saha, K. Rashid, P. Sadhukhan, N. Agarwal, P.C. Sil, Biofactors 42 (2016) 515.
[45] K. Sinha, P. Sadhukhan, S. Saha, P.B. Pal, P.C. Sil, Biochimica et Biophysica Acta (BBA)-General Subjects 1850 (2015) 769.
[46] J. Das, V. Vasan, P.C. Sil, Toxicol. Appl. Pharmacol. 258 (2012) 296.
[47] P. Sadhukhan, S. Saha, K. Sinha, G. Brahmachari, P.C. Sil, PLoS One 11 (2016) 1.
[48] E.I. Stiefel, Prog. Inorg. Chem. 22 (1977) 1.
[49] M.R. Maurya, N. Saini, F. Avecilla, Polyhedron 90 (2015) 221.
[50] M. Cindrić, V. Vrdoljak, T.K. Novak, N. Strukan, A.B.- Saranović, P. Novak, B. Kamenar, Polyhedron 23 (2004) 1859.
[51] Y.-L. Zhai, X.-X. Xu, X. Wang, Polyhedron 11 (1992) 415.
[52] M. Cindric, V. Vrdoljak, T. Kajfez, P. Novak, A.B.- Saranovic, N. Strukan, B. Kamenar, Inorg. Chim. Acta 328 (2002) 23.
[53] H.K. Saha, A. Saha, S.S. Mandal, J. Indian Chem. Soc. (1984) 902.
[54] E. Kahrović, K. Molčanov, L. T-Bozić, B. K-Prodić, Polyhedron 25 (2006) 2459.
[55] H.K. Saha, B.K. Sikdar, T.K. Raychaudhuri, J. Indian Chem. Soc. 11 (1982) 723.
[56] S.R. Girish, V.B. Mahale, Trans. Met. Chem. 16 (1991) 435.
[57] P. Alonso, I. Frutos, T. Gulierrez, A.D. Lopez, Trans. Met. Chem. 12 (1987) 133.
[58] H.K. Saha, M.C. Halder, J. Inorg. Nucl. Chem. 34 (1972) 3097.
[59] H.K. Saha, A.K. Banerjee, J. Inorg. Nucl. Chem. 34 (1972) 1861.
[60] M.C. Baired, Prog. Inorg. Chem. 9 (1968) 29.
[61] C.J. Doonan, C. Gourlay, D.J. Nielsen, V.W.L. Ng, P.D. Smith, D.J. Evans, G.N. George, J.M. White, C.G. Young, Inorg. Chem. 54 (2015) 6386.
[62] Y. Okubo, A. Okamura, K. Imanishi, J. Tachibana, K. Umakoshi, Y. Sasaki, T. Imamura, Bull. Chem. Soc. Jpn. 72 (1999) 2241.
[63] T. Kojima, R. Harada, T. Nakanishi, K. Kaneko, S. Fukuzumi, Chem. Mater. 19 (2007) 51.
[64] M.B. Hursthouse, W. Levason, R. Ratnani, G. Reid, Polyhedron 23 (2004) 1915.
[65] C.D. Garner, N.C. Howlader, F.E. Mabbs, J. C. S. Dalton. (1978) 1848.
[66] L.M.R. Jensen, B.F. Abrahams, C.G. Young, J. Coord. Chem. 66 (2013) 1252.
[67] V. Vrdoljak, B. Progovecki, D. Matkovic-Calogovic, P. Novak, M. Cindric, Inorg. Chim. Acta 363 (2010) 3516.
[68] B. Kamenar, B. Korpar-Colig, M. Penavic, M. Cindric, J. C. S. Dalton. Trans. (1990) 1125.
[69] S. Saha, R. Majumdar, M. Roy, R.R. Dighe, A.R. Chakravarty, Inorg. Chem. 48 (2009) 2652.
[70] L. Li, Q. Guo, J. Dong, T. Xu, J. Li, J. Photochem. Photobiol. B 125 (2013) 56.
[71] N. Busto, J. Valladolid, M. Martínez-Alonso, H. J. Lozano, F. A. Jalon, B. R. Manzano, A. M. Rodríguez, M. Carmen Carrión, TaritaBiver, J. M. Leal, G. Espino, B. García, Inorg. Chem. 52 (2013) 9962.
[72] P. Krishnamoorthy, P. Sathyadevi, A.H. Cowley, R. Butorac, N. Dharmaraj, Eur. J. Med. Chem. 46 (2011) 3376.
[73] P. Sathyadevi, P. Krishnamoorthy, R. Butorac, A.H. Cowley, N.S.P. Bhuvanesh, N. Dharmaraj, Dalton Trans. 40 (2011) 9690.
[74] P. Krishnamoorthy, P. Sathyadevi, A.H. Cowley, R. Butorac, N. Dharmaraj, Dalton Trans. 41 (2012) 6842.
[75] D. Senthil Raja, N.S.P. Bhuvanesh, K. Natarajan, Eur. J. Med. Chem. 46 (2011) 4584.
[76] G. Cohen, H. Eisenberg, Biopolymers 8 (1969) 45.
[77] M.L. Harikumaran Nair, D. Thankamani, Indian J. Chem. 48A (2009) 1212.
[78] B.S. Sekhon, L. Gandhi, Resonance 1 (2006) 75.
[79] J.D. Knoll, C. Turro, Coord. Chem. Rev. 282-283 (2015) 110.